RESEARCH/REVIEW ARTICLE

Dolerites of Svalbard, north-west Barents Sea Shelf: age, tectonic setting and significance for geotectonic interpretation of the High-Arctic Large Igneous Province

Krzysztof Nejbert[1], Krzysztof P. Krajewski[2], Elżbieta Dubińska[1] & Zoltán Pécskay[3]

[1] Institute of Geochemistry, Mineralogy and Petrology, University of Warsaw, Al. Żwirki i Wigury 93, PL-02089 Warsaw, Poland
[2] Institute of Geological Sciences, Polish Academy of Sciences, Research Centre in Warsaw, ul. Twarda 51/55, PL-00818 Warsaw, Poland
[3] Institute of Nuclear Research, Hungarian Academy of Sciences, Bem tér 18/c, HU-4026 Debrecen, Hungary

Keywords
Dolerite; geochemistry; petrogenesis; K–Ar whole rock ages; Svalbard; Cretaceous.

Correspondence
Krzysztof P. Krajewski, Institute of Geological Sciences, Polish Academy of Sciences, Research Centre in Warsaw, ul. Twarda 51/55, PL-00818 Warsaw, Poland. E-mail: kpkraj@twarda.pan.pl

Abstract

The dolerites of Svalbard are mineralogically and geochemically homogeneous with geochemical features typical of continental within-plate tholeiites. Their geochemistry is similar to tholeiites belonging to a bimodal suite defined as the High-Arctic Large Igneous Province (HALIP). K–Ar dating of numerous dolerites sampled from many locations across Svalbard define a narrow time span of this magmatism from 125.5 ± 3.6 to 78.3 ± 2.6 Mya. Discrete peaks of intensive activity occurred at 115.3, 100.8, 91.3 and 78.5 Mya corresponding to (1) breakup of the continental crust and formation of an initial rift as a result of mantle plume activity, located in the southern part of the Alpha Ridge; (2) magmatic activity related to spreading along the Alpha Ridge that led to the development of the initial oceanic crust and (3) continuation of spreading along the Alpha Ridge and termination of magmatic activity related to HALIP (last two peaks at 91.3 and 78.5 Mya).

A widespread Late Mesozoic thermal event in the Arctic has been identified as forming the High-Arctic Large Igneous Province (HALIP), with evidence of its existence in Svalbard, Franz Josef Land and the adjacent shelf areas, the Canadian Arctic Archipelago and northern Greenland (Tarduno 1998; Maher 2001). These areas were peripheral during the development of the Amerasian Basin and the Alpha Ridge (Fig. 1). Magmatism in HALIP covered an area of several hundred thousand square kilometres, showing variability in the styles and timing of activity peaks. The origin and conditions of the formation of HALIP are subjects of scientific debate, though current evidence points to its development as a result of the activity of a mantle plume. However, alternative models have been suggested for large igneous provinces in general (Ernst et al. 2005; Saunders 2005; Bryan & Ernst 2007), including delamination, meteorite impact, small-scale rift-related convection and chemical mantle heterogeneities. Clearly, further data on the geology, geochemistry and geochronology of the magmatic bodies are needed to improve our understanding of the HALIP's origin.

HALIP rocks are difficult to access, hence knowledge of the magmatism is still limited. The dolerites of Svalbard are a notable component of the province and the petrological and geochronological data presented in this research substantially broaden our knowledge of their petrogenesis. This paper elucidates the origin and the age of Late Mesozoic magmatic intrusions in Svalbard on the basis of detailed petrographic and geochemical analysis and a new set of K–Ar age determinations.

Geological setting

Svalbard is the emergent north-western corner of the Barents Sea Shelf (Fig. 1), bordered on the north by a passive continental margin towards the Arctic Ocean and on the west by the spreading axis of the Knipovich Ridge (Talvani & Eldholm 1977). The islands of Svalbard, including Spitsbergen, Nordaustlandet,

Citation: *Polar Research* 2011, *30*, 7306, DOI: 10.3402/polar.v30i0.7306

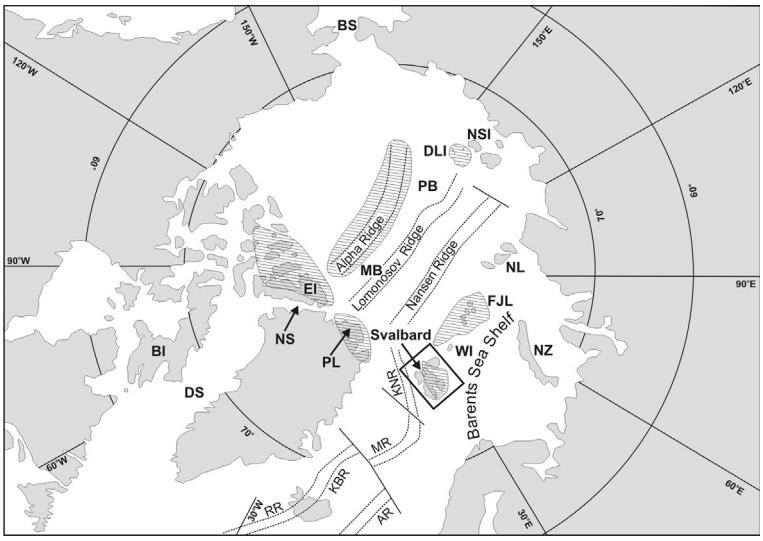

Fig. 1 Map of the Arctic landmasses showing the location of Svalbard and areas (hatched fields) with occurrences of the igneous rocks of the High-Arctic Large Igneous Province. The map is based on the general map of the Arctic compiled by Harland (1997) and data from Bailey & Rasmussen (1997), Maher (2001), Kontak et al. (2001) and Jones et al. (2007). Geographical features shown are Aegir Ridge (AR), Baffin Island (BI), Bering Strait (BS), Davis Strait (DS), De Long Islands (DLI), Ellesmere Island (EI), Franz Josef Land (FJL), Kolbeinsey Ridge (KBR), Knipovich Ridge (KNR), Makarov Basin (MB), Mohns Ridge (MR), New Siberian Islands (NSI), Northern Land (NL), Nares Strait (NS), Novaya Zemlya (NZ), Podvodnikov Basin (PB), Perry Land (PL), Reykjanes Ridge (RR) and White Island (WI).

Edgeøya, Barentsøya and many others (Fig. 2), were uplifted by Late Mesozoic and Cenozoic crustal movements, providing insight into the deeper geological structure of the region and the stratigraphic column from Paleoproterozoic to Paleogene times (Harland 1997; Dallmann et al. 2002). The Caledonian basement (Paleoproterozoic through Ordovician) hosts tectonic depressions filled by the Devonian Old Red Sandstone (Andrée Land Group) and is covered by a single sedimentary complex of Late Paleozoic and Mesozoic platform strata. This complex is subdivided into six groups occurring in stratigraphic order: the Late Paleozoic (1) Billefjorden, (2) Gipsdalen and (3) Tempelfjorden groups; and the Mesozoic (4) Sassendalen, (5) Kapp Toscana and (6) Adventdalen groups (Dallmann 1999).

The opening of the Arctic and North Atlantic oceans in Paleogene time and the interdependent stages of separation of Svalbard and Greenland shaped the present tectonic structure of Svalbard. A thrust-and-fold belt stretches along western Spitsbergen, owing its origin to a dextral plate transform setting with strike-slip and convergent movements (Maher & Craddock 1988). The belt is bordered on the east by the simultaneously formed Central Spitsbergen Basin (Paleogene succession), which passes eastwards into Eastern Svalbard Platform (Mesozoic succession). The reverse uplift of the western Spitsbergen orogen and northern Spitsbergen and northern Nordaustlandet resulted there in the erosion of younger strata and the exposure of the Caledonian basement and Devonian through Permian successions.

The Late Mesozoic magmatism is represented by extensive dolerite intrusions in Spitsbergen, Nordaustlandet, Edgeøya and Barentsøya and along Hinlopenstretet and by extrusives in Kong Karls Land in easternmost Svalbard (Fig. 2). These magmatic bodies are known as the Diabasodden Suite in the local lithostratigraphic scheme, with the stratotype defined at Diabasodden on the southern margin of Isfjorden/Sassenfjorden in central Spitsbergen (Dallmann 1999). Two areas show a concentration of the magmatic bodies: the eastern Svalbard dolerite belt and the central Spitsbergen dolerite centre. The eastern dolerite belt stretches from the small islands of Tusenøyane in the south, through western Edgeøya, Barentsøya, Olav V Land in Spitsbergen, the islands in Hinlopenstretet, to western Nordaustlandet. Isolated intrusions also occur further north on Nordaustlandet and on Lågøya. The dolerite centre in Spitsbergen embraces magmatic bodies occurring around inner Isfjorden, Sassenfjorden, Billefjorden and Dicksonfjorden. Extensive bodies also occur in eastern Sabine Land, though it is not clear whether they continue under Storfjorden to join the eastern belt. Magnetic anomalies also suggest the

Citation: *Polar Research* 2011, *30*, 7306, DOI: 10.3402/polar.v30i0.7306

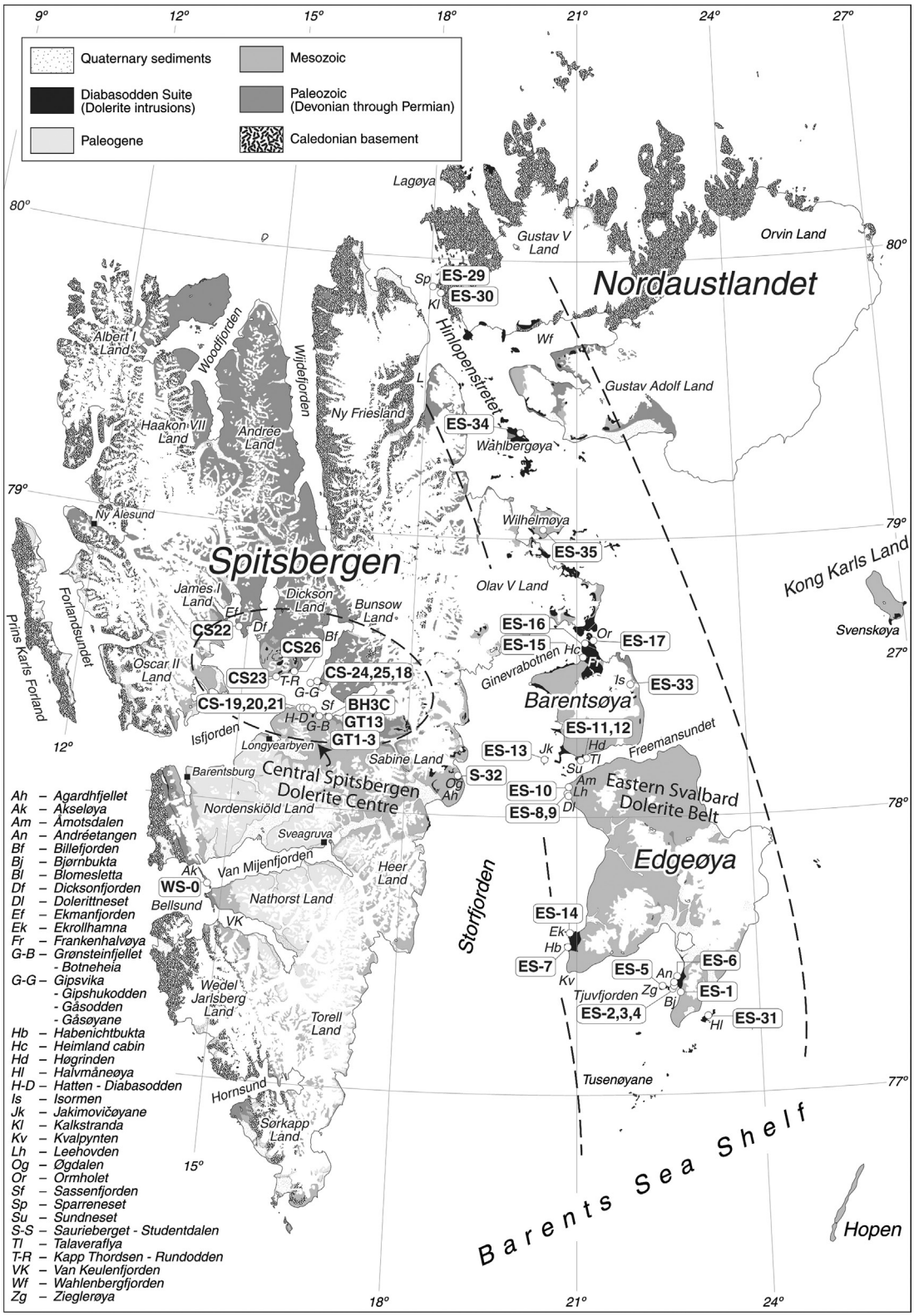

Fig. 2 Geological map of Svalbard showing the distribution of dolerite intrusions (Diabasodden Suite) and the locations where samples analysed in this paper were collected. The map is based on Dallmann et al. (2002).

presence of widespread dolerite bodies located south and east of Svalbard on the Barents Sea Shelf (Grogan et al. 2000). The total area of dolerite occurrences in the north-west Barents Sea Shelf is approximately 200 000 km^2 and their minimum volume is estimated at 10 000 km^3 (Maher 2001).

The dolerite intrusions are mainly sills with subordinate dykes (Fig. 3, 4). The vast majority of sills occur in the Mesozoic (Triassic through Early Cretaceous) and less commonly in the Late Paleozoic sedimentary formations. Thermal metamorphism of the host rocks along the sill margins is usually observed, particularly in the Triassic and Jurassic organic carbon-rich shales and mudstones. The alteration zones are usually thin (0.1–0.5 m), attaining a maximum of 6 m along extremely thick sills.

The sills vary in thickness from less than 1 m to more than 100 m, although most of them are about 10 to 30 m thick. Their morphology varies between sills and within the sills. Three varieties can be distinguished: (1) horizontal sills, (2) undulating sills and (3) climbing sills. Where observed in stacked sills on mountain slopes, the climbing sills may join the overlying ones at low angles. Thin vertical to subvertical dykes also provide junctions between superimposed sills. The sills may terminate laterally by a decrease in thickness or transform abruptly into dykes. Although rare in Svalbard, dolerite dykes more commonly occur in the Caledonian basement than in the overlying succession (Birkenmajer & Morawski 1960; Dallmann et al. 1993). Within the Paleogene Spitsbergen thrust-and-fold belt, they are tectonically disturbed as a rule (Birkenmajer 1986), whereas in the basement of northern Svalbard such deformation has not been observed. The general pattern of dolerite intrusions and their morphological variations suggest that the dykes occurring in the basement and older formations represent a root part of the intrusive system, whereas thick, recurrent sills in the Mesozoic formations can be considered its finger-like

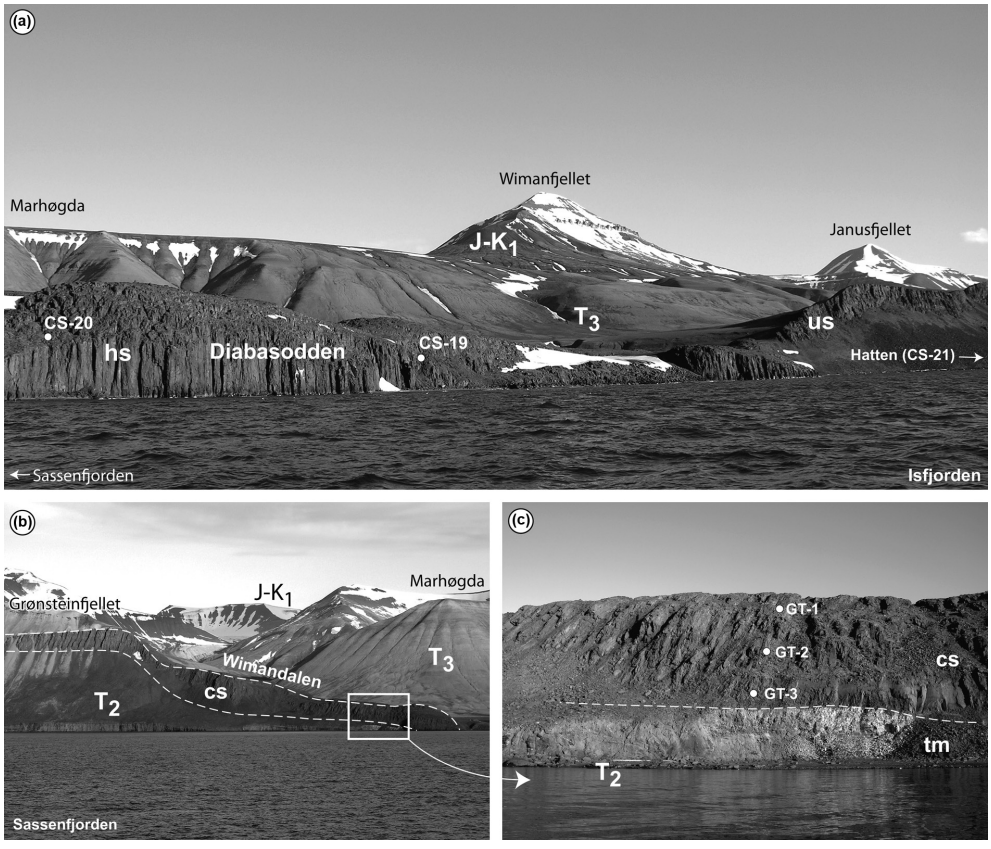

Fig. 3 Examples of dolerite intrusions in the central Spitsbergen dolerite centre. (a) Undulating sill (us) overlapping a thick horizontal sill (hs) between Hatten and Diabasodden at the southern margin of Isfjorden/Sassenfjorden (stratotype for the Diabasodden Suite). (b) Thick climbing sill (cs) at Grønsteinfjellet (southern margin of Sassenfjorden). (c) Enlarged part of the climbing sill (cs), showing the thick thermal alteration zone (tm) developed in the Triassic organic carbon-rich shales. Sampling locations and stratigraphy of the hosting rocks are indicated in all three images.

Citation: *Polar Research* 2011, *30*, 7306, DOI: 10.3402/polar.v30i0.7306

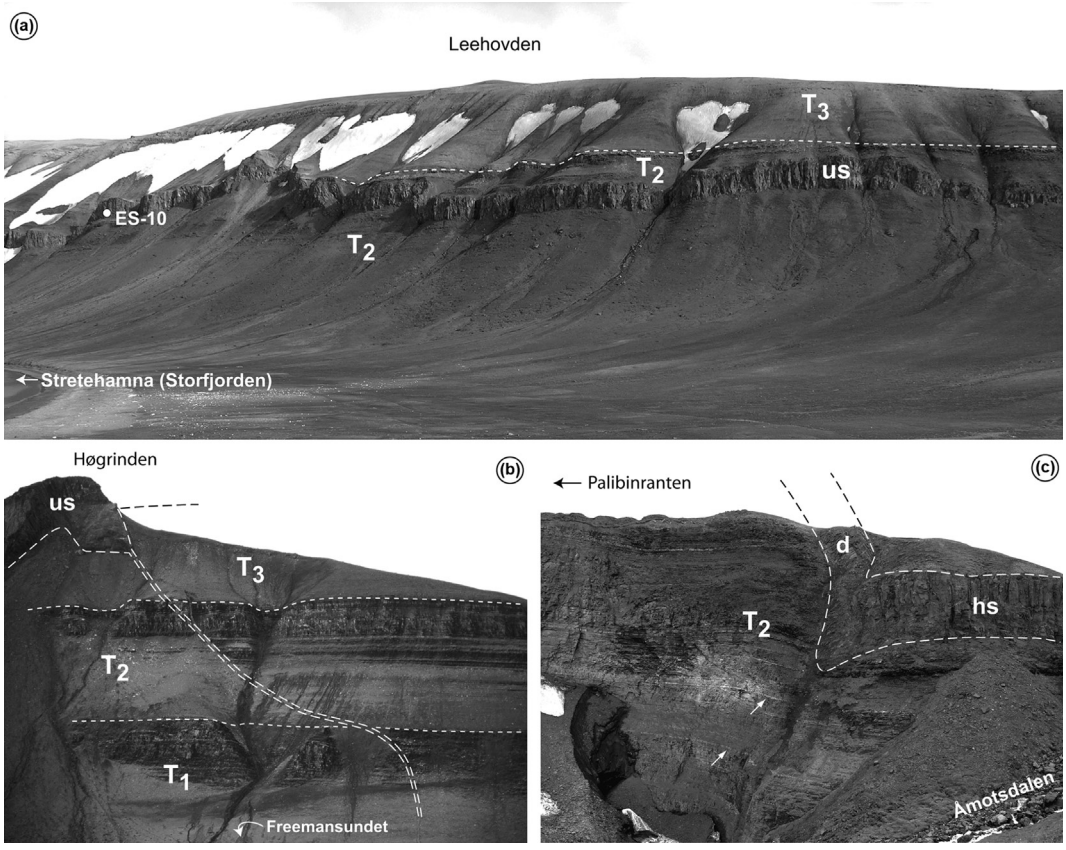

Fig. 4 Examples of dolerite intrusions in the eastern Svalbard dolerite belt. (a) Undulating sill (us) in the Triassic shale succession exposed along western slope of Leehovden, north-western Edgeøya. (b) Thin subvertical dyke cutting the Triassic shale succession, exposed on southern slope of Høgrinden, southern Barentsøya. The dyke terminates in a thick undulating sill (us). (c) Horizontal sill (hs) abruptly changing into a dyke at Åmotsdalen, north-western Edgeøya. Note the undisturbed bed succession of the Triassic organic carbon-rich rocks below the abrupt change of intrusion morphology (arrows). Sampling locations and stratigraphy of the hosting rocks are indicated in all three images.

upper termination. This cannot be documented with certainty, because a continuous vertical section of the system from the basement to the Mesozoic formations is not exposed. The dominance of dykes in the basement and sills in overlying Mesozoic formations indicate a extensional tectonic regime in Svalbard. This is consistent with the presence of a large radiating dyke swarm recognized in the Canadian Arctic (Buchan & Ernst 2006) and in Franz Josef Land (Dibner 1998), which was later divided by plate tectonic processes related to the opening of the North Atlantic Ocean. The depth of emplacement of sill intrusions in western Spitsbergen has been estimated at 1–2 km (Maher 2001). This depth shallows eastwards, dropping to nil in Kong Karls Land, where basaltic lava flows appear in the Cretaceous succession (Smith et al. 1976).

The age of dolerite intrusions in Svalbard has been debated since the first attempt of radiometric dating by Gayer et al. (1966). This and subsequent approaches (Burov et al. 1977; Vincenz et al. 1981; Birkenmajer et al. 2010) are discussed below vis-à-vis the dates we obtained. There are, however, some lines of geological evidence that may be conclusive in this respect. On the basis of biostratigraphic data and analysis of unconformities in the sedimentary succession, Parker (1966, 1967) demonstrated that some dolerites intruded between the deposition of the Agardhfjellet Formation (Late Jurassic) and the Rurikfjellet Formation (Berriasian–Barremian). From a petrographic analysis of the Carolinefjellet Formation (Aptian–Albian), Maher (2001) documented a widespread Aptian transition from quartz arenites to lithic arenites and feldspathic sandstones, reflecting new volcanic sources of clastic material in Svalbard. This points to at least two peaks of intrusive activity that correlate with two regional regressive trends and related unconformities in the Cretaceous succession. These regressive trends (Barremian and Albian), which are inconsistent with global sea-level changes, suggest

the existence of thermal domes related to magmatic activity (Maher 2001).

Samples

Thirty-nine samples of Svalbard dolerites were collected for this study (Table 1; Fig. 2). Twenty-three samples represent the eastern Svalbard dolerite belt (ES-1–17, 29–31, 33–35) and 14 samples are from the central Spitsbergen dolerite centre (CS-18–26, GT-1–3, GT-13, BH-3C). One dolerite sample (WS-0) from the western Spitsbergen thrust-and-fold belt and one from eastern Spitsbergen (S-32) were analysed as well (Fig. 2).

Dolerite sills occurring on the eastern side of Tjuvfjorden on the island of Edgeøya and in the Tusenøyane islands are represented by samples ES-1–6 and ES-31. The main horizontal sill at Andréetangen was sampled at three points from north to south (ES-2–4). It is likely that this sill extends westward and crops out on the neighbouring islands, where a sample (ES-5) was taken on western coast of Zieglerøya. Sample ES-1 is from a thin subvertical dyke located in Bjørnbukta south of Andréetangen and sample ES-6 from an isolated sill at its northern margin. The island of Halvmåneøya is part of a thick sill, where lower contact is not exposed. Sample ES-31 was taken from the middle of the northern cliff of the island. The dolerite cluster north of Kvalpynten in south-west Edgeøya contains at least two large horizontal sills, which were sampled in Habenichtbukta (ES-7, southern sill) and in Ekrollhamna (ES-14, northern sill). Dolerite sills that crop out in north-western Edgeøya, south-west Barentsøya and on the neighbouring small islands in Storfjorden were sampled at six locations. Samples ES-8 and ES-9 represent an undulating sill exposed at Dolerittneset and sample ES-10 comes from an undulating sill on the western slope of Leehovden in north-west Edgeøya (Fig. 4a). Two sills exposed towards Freemansundet in south-west Barentsøya were sampled at Talaveraflya (ES-11) and Sundneset (ES-12). Small islands in Storfjorden at the entrance to Freemansundet are likely to represent fragments of one large horizontal sill, with only the upper part being exposed above sea level. Sample ES-13 was collected on the eastern coast of the northern island of the Jakimovičøyane archipelago. The dolerite cluster occurring on both sides of Ginevrabotnen (northern Barentsøya and Olav V Land in Spitsbergen) is the biggest exposed intrusive body in Svalbard. In northern Barentsøya, it is represented by an extensive sill of a horizontal to slightly undulating morphology that crops out over several square kilometres in Frankenhalvøya. Three samples were collected in this area: the coastal cliff north of Heimland cabin (ES-15) and the western (ES-16) and eastern (ES-17) mouth of the Ormholet canyon. In eastern Barentsøya, the topmost sill in the Kapp Toscana sedimentary sequence was sampled on Isormen (ES-33). Samples from sills in Wilhelmøya and Wahlbergøya islands in Hinlopenstretet were collected by Dr Atle Mørk and kindly provided to us for analysis. On Wilhelmøya, the topmost sill that caps the Kapp Toscana succession was sampled (ES-35). Most of Wahlbergøya is made up of a thick horizontal sill that was sampled in the north-eastern coastal cliff (ES-34). In western Nordaustlandet, two vertical dolerite dykes cutting the Caledonian basement (Neoproterozoic Roaldtoppen Group) were sampled in coastal exposures at Sparreneset (ES-29) and Kalkstranda (ES-30).

In the central Spitsbergen dolerite centre, samples were collected at four locations: (1) in the stratotype area at the southern margin of Isfjorden/Sassenfjorden, (2) between Gipsvika and Gåsøyane at the entrance to Billefjorden, (3) between Kapp Thordsen and Rundoddden at the northern margin of Isfjorden and (4) at the eastern side of Ekmanfjorden. Two samples were collected from a thick horizontal sill at Diabasodden (CS-19, 20), from the western and eastern side of the headland point, respectively (Fig. 3a). A third sample (CS-21) was collected at Hatten from an undulating sill that continues westwards from Diabasodden. Five samples were collected from sills located east of Diabasodden: three (GT1-3) from a thick climbing sill, one (GT-13) from a thin vertical dyke at Grønsteinfjellet and one from a thin sill in eastern Botneheia (BH-3C). Samples GT1-3 represent a vertical section through the sill (Fig. 3b, c). The dolerite intrusion at the eastern entrance to Billefjorden consists of a thick horizontal to slightly climbing sill that is exposed along the coast of Isfjorden and transforms up the slope of Gipshuken into a subvertical dyke. Two samples—one from the south-eastern termination of the outcrop belt at Gipshukodden (CS-18) and one from the north-western termination at Gåsodden (CS-25)—were collected. The islands of Gåsøyane located further westward consist of a thick horizontal sill that is likely to be a continuation of the Gipshukodden–Gåsodden sill. One sample representing the upper part of the sill was collected from the eastern coast of the island Gåsøya (CS-24). Two samples were collected from coastal exposures between Billefjorden and Nordfjorden. One sample represents a thick sill that climbs north-eastwards from the coast east of Kapp Thorsden up the slope of Saurieberget (CS-23). The other was taken from a subvertical dyke located east of Kapp Thordsen at the mouth of Studentdalen (CS-26). In Ekmanfjorden, a part of a thick undulating sill is exposed along Blomesletta. A

Citation: *Polar Research* 2011, *30*, 7306, DOI: 10.3402/polar.v30i0.7306

Table 1 Details of samples from eastern Svalbard (sample numbers starting with ES), central Spitsbergen (numbers starting with CS as well as samples GT–1-3, GT–13 and BH-3C), western Spitsbergen (WS) and eastern Spitsbergen (S).

Sample no.	Locality	GPS coordinates	Sample represents	Hosting rock
ES-1	Bjørnbukta, Edgeøya	N77 22.141 E22 42.100	Thin subvertical dyke, central part	Kapp Toscana Group (T3)
ES-2	Andréetangen (I), Edgeøya	N77 23.640 E22 35.389	Horizontal to undulated sill, central part	Kapp Toscana Group (T3)
ES-3	Pongtongen (I), Edgeøya	N77 23.539 E22 35.256	Horizontal to undulated sill, central part	Kapp Toscana Group (T3)
ES-4	Pongtongen (II), Edgeøya	N77 23.138 E22 34.574	Horizontal to undulated sill, central part	Kapp Toscana Group (T3)
ES-5	Zieglerøya, Tjuvfjorden	N77 23.311 E22 23.591	Horizontal sill, central part	Kapp Toscana Group (T3)
ES-6	Andréetangen (II), Edgeøya	N77 25.424 E22 39.288	Horizontal to undulated sill, central part	Kapp Toscana Group (T3)
ES-7	Habenichtbukta, Edgeøya	N77 32.139 E20 51.120	Thick horizontal sill, central part	Kapp Toscana Group (T3)
ES-8	Dolerittneset (I), Edgeøya	N78 04.655 E20 49.096	Undulated sill, upper part	Sassendalen Group (T1–T2)
ES-9	Dolerittneset (II), Edgeøya	N78 04.881 E20 48.159	Undulated sill, upper part	Sassendalen Group (T1–T2)
ES-10	Leehovden, Edgeøya	N78 05.372 E20 49.342	Undulated sill, central part	Sassendalen Group (T1–T2)
ES-11	Talaveraflya, Barentsoya	N78 12.989 E21 09.198	Thick horizontal sill, central part	Sassendalen Group (T1–T2)
ES-12	Sundneset, Barentsøya	N78 12.249 E21 03.833	Thick horizontal sill, upper part	Sassendalen Group (T1–T2)
ES-13	Jakimovičøyane, Storfjorden	N78 13.020 E20 27.743	Horizontal sill, upper part	Sassendalen Group (T1–T2)
ES-14	Ekrollhamna, Edgeøya	N77 34.867 E20 52.947	Thick horizontal sill, central part	Sassendalen Group (T1–T2)
ES-15	Heimland, Barentsøya	N78 35.562 E21 06.651	Thick undulated sill, central part	Sassendalen–Kapp Toscana groups (T)
ES-16	Ormholet (W), Barentsøya	N78 37.532 E21 09.010	Thick horizontal sill, central part	Sassendalen–Kapp Toscana groups (T)
ES-17	Ormholet (E), Barentsøya	N78 37.853 E21 17.507	Thick horizontal sill, central part	Sassendalen–Kapp Toscana groups (T)
CS-18	Gipshukodden, Spitsbergen	N78 26.016 E16 24.779	Thick horizontal sill, central part	Gipsdalen Group (C)
CS-19	Diabasodden (W), Spitsbergen	N78 21.808 E16 07.699	Thick horizontal to undulated sill, central part	Kapp Toscana Group (T3)
CS-20	Diabasodden (E), Spitsbergen	N78 21.745 E16 09.139	Thick horizontal to undulated sill, central part	Kapp Toscana Group (T3)
CS-21	Hatten, Spitsbergen	N78 21.550 E16 02.731	Thick undulated sill, central part	Kapp Toscana Group (T3)
CS-22	Blomesletta, Spitsbergen	N78 37.068 E14 49.644	Thick undulated sill, central part	Gipsdalen Group (C)
CS-23	Kapp Thordsen (W), Spitsbergen	N78 27.488 E15 35.112	Thick climbing sill, central part	Sassendalen Group (T1-T2)
CS-24	Gåsøyane, Spitsbergen	N78 27.201 E16 13.557	Thick horizontal to climbing sill, upper part	Gipsdalen Group (C)
CS-25	Gåsodden, Spitsbergen	N78 27.380 E16 17.689	Thick horizontal to climbing sill, upper part	Gipsdalen Group (C)
CS-26	Kapp Thordsen (E), Spitsbergen	N78 28.688 E15 52.541	Thin climbing sill, central part	Tempelfjorden Group (P)
WS-0	Akseløya, Spitsbergen	No GPS data	Thin subvertical dyke, central part	Tempelfjorden Group (P)
GT-1	Grønsteinfjellet, Spitsbergen	N78 21.265 E16 11.792	Thick climbing sill, upper part	Sassendalen–Kapp Toscana groups (T)
GT-2	Grønsteinfjellet, Spitsbergen	N78 21.265 E16 11.792	Thick climbing sill, central part	Sassendalen–Kapp Toscana groups (T)
GT-3	Grønsteinfjellet, Spitsbergen	N78 21.265 E16 11.792	Thick climbing sill, lower part	Sassendalen–Kapp Toscana groups (T)
GT-13	Grønsteinfjellet, Spitsbergen	N78 21.039 E16 13.344	Thin vertical dyke, central part	Sassendalen Group (T1–T2)
BH-3C	Botneheia (E), Spitsbergen	N78 18.997 E16 30.493	Thin horizontal sill, lower part	Sassendalen Group (T1–T2)
ES-29	Sparreneset, Nordaustlandet	N79 53.599 E18 11.041	Vertical dyke, central part	Roaldtoppen Group (Proterozoic)
ES-30	Kalkstranda, Nordaustlandet	N79 53.063 E18 11.841	Vertical dyke, central part	Roaldtoppen Group (Proterozoic)
ES-31	Halvmåneøya, SE of Edgeøya	N77 16.781 E23 06.796	Thick horizontal sill, upper part	Kapp Toscana Group (T3)
S-32	Øgledalen, Spitsbergen	N78 06.269 E18 59.752	Subvertical dyke, central part	Adventdalen Group (J-K1)
ES-33	Isormen, Barentsøya	N78 26.214 E22 03.705	Horizontal sill, lower part	Kapp Toscana Group (T3)
ES-34	Wahlbergøya, Hinlopenstretet	No GPS data	Thick undulated sill, central part	Tempelfjorden Group (P)
ES-35	Wilhelmøya, Hinlopenstretet	No GPS data	Thick horizontal sill, central part	Kapp Toscana Group (T3-J1)

sample was taken from the southern coastal outcrop of the sill (CS-22).

A sample from the western Spitsbergen thrust-and-fold belt was taken from a subvertical dyke cutting the Permian Kapp Starostin Formation on western shore of Akseløya (WS-0). In eastern Spitsbergen, a subvertical dyke cutting the Upper Jurassic black shales of the Agardhfjellet Formation was sampled in Øgledalen north of Agardhfjellet (S-32).

Analytical methods

Mineral compositions in the dolerites were determined using a SX 100 electron probe micro-analyser (CAMECA, Gennevilliers, France) at the Inter-Institute Analytical Complex for Minerals and Synthetic Substances at Warsaw University. These analyses were made under the following instrumental conditions: accelerating voltage 15 keV, beam current 20 nA and beam diameter 1 μm. Natural and synthetic materials distributed by CAMECA and SPI Supplies (West Chester, PA, USA) were used as the calibration standards. Maps of the distribution of elements within the fine-grained groundmass were prepared using a JSM-6380 LA scanning electron microscope (JEOL, Tokyo, Japan) at the Scanning Electron Microscope and Microanalysis Laboratory at Warsaw University. The total time of acquisition of one set of these maps recorded from one area was up to 14 h.

Major and trace element abundances were determined at Acme Analytical Laboratories Ltd in Vancouver, BC, Canada. The samples were sent to the laboratory in two separate sample-sets about one year apart. The quality of the material for analyses was checked under a binocular microscope and only fresh rock free of weathering and traces of alteration was used for geochemical investigation. The major elements, Ni and Sc were analysed by inductively coupled plasma emission spectrometry (ICP-ES), while trace elements, including rare earth elements (REE), were analysed by inductively coupled plasma mass spectroscopy (ICP-MS). All samples for analysis were prepared by fusion of 0.2 g of the sample with a mixture of $LiBO_2$ and $Li_2B_4O_7$. The calibration standards SO-18/CSC and SO-18 were applied during ICP-ES and ICP-MS studies, respectively. Standard procedures commonly used during determination of chemical composition at Acme Analytical Laboratories were applied. Results of chemical determination of two reference materials SO-18/CSC and SO-18, together with duplicated analyses of samples ES-7 and BH-3B, were used to check the accuracy and precision of the results.

The K–Ar study was carried out at the Institute of Nuclear Research of the Hungarian Academy of Sciences (Debrecen, Hungary). A piece of about 1 kg, free of weathering, xenoliths and joints, was crushed to obtain small chips of dolerites (up to 0.5 cm in diameter) and then unaltered chips were selected for the study using stereoscopic microscope. After final crushing, approximately 100 g of the 150–300 μm size fraction was separated using copper sieves. A small portion of this material taken from each separate was ground in an agate mortar and used for potassium analyses. K–Ar datings were made on whole rocks samples, the mineralogy and texture of the investigated magmatic rocks being unsuitable for mineral separation.

To determine the potassium content, powder samples were digested in acids (HF, HNO_3 and H_2SO_4) in teflon beakers and finally dissolved in 0.2 M HCl and later analysed for potassium by flame photometry with Na buffer and Li internal standard. Multiple runs of inter-laboratory standards (LP-6, HD-B1, GL-0 and Asia 1/65) indicated the accuracy and reproducibility of this method to be within 2%.

To measure argon, approximately 0.2–0.3 g of samples were wrapped in a copper sieve, preheated for about 24 h at 150 °C in high vacuum line and then degassed using induction heating. St 707 getter material (SAES Getters, Milan; Italy) and cold traps were used for gas cleaning and transporting of Ar. The isotopic composition of the argon was measured by isotope dilution with ^{38}Ar tracer and 15-cm radius magnetic sector type mass spectrometer was used in the static regime. Atomic constants suggested by Steiger & Jager (1977) were used for calculating ages. All analytical errors represent one standard deviation (1σ, 68% confidence level). Details of the instruments, the applied methods and results of calibration have been described elsewhere (Dalrymple & Lanphere 1969; Balogh 1985).

Petrography of dolerites

The Svalbard dolerites are black and mostly fine-grained with crystals up to 5 mm. Most samples are slightly texturally variable (Fig. 5), being composed of medium- to fine-grained rock types showing doleritic and, less commonly, ophitic texture. Thick sills may show coarse-grained, ophitic and/or subophitic texture in their central parts (Fig. 5a, b) and doleritic texture toward their margins (Fig. 5c). Doleritic texture is also most common within thin dolerite dykes. Sill margins are extremely fine-grained and slightly porphyritic (Fig. 5d). Patches of extremely fine-grained mesostasis (Fig. 6), randomly distributed within a thin section and consisting of skeletal crystals of feldspars, clinopyroxene, Fe–Ti oxides and apatite are commonly observed. In some patches only

Citation: *Polar Research* 2011, *30*, 7306, DOI: 10.3402/polar.v30i0.7306

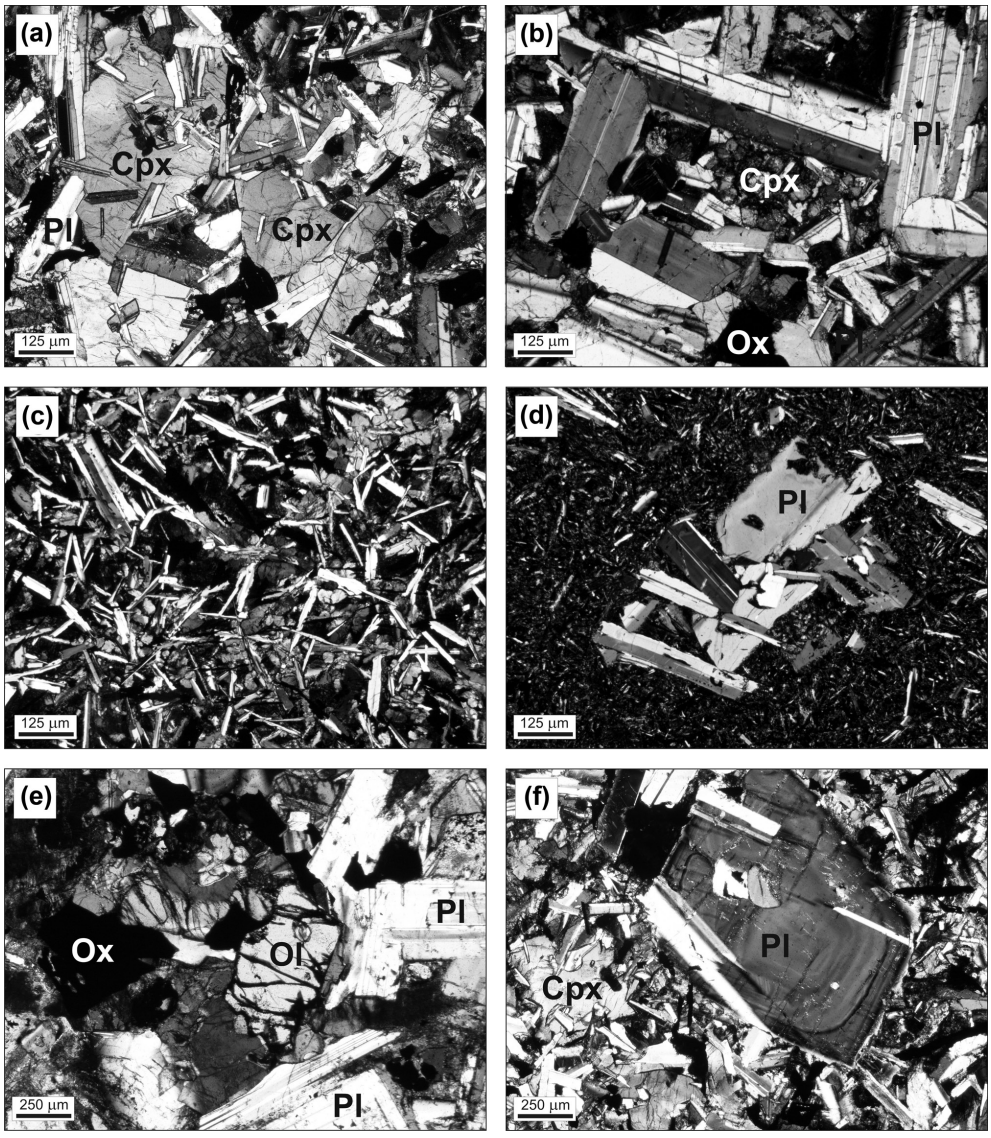

Fig. 5 Petrography of the major dolerite types in Svalbard. (a) Ophitic texture; sample ES-13. (b) Intersertal (diabasic) texture; sample ES-29. (c) Fine-grained, intersertal texture; sample BH-3C. (d) Fine-grained with plagioclase agglomerate, typical for chilled zones and thin dolerite dykes, sample BH-3A. (e) Coarse-grained dolerite with olivine phenocryst; sample ES-16. (f) Plagioclase phenocryst within coarse grained dolerite; sample ES-3A. The photographs were taken with transmitted light, crossed nicols. Grains of clinopyroxene (Cpx), olivine (Ol), oxides (Ox) and plagioclase (Pl) are indicated.

devitrified glass and skeletal Fe–Ti oxides are seen. Amygdales filled with secondary Ca–Mg–Fe carbonates intergrown with clay minerals are found in marginal parts of the sills.

Three genetically different components within the dolerite are recognized: (1) phenocrysts (Fig. 5f); (2) minerals that grew from the melt after their final emplacement into sills, represented by plagioclase framework where interstitial spaces are filled by later clinopyroxene (Fig. 5a, b, e) and (3) secondary minerals reflecting late alteration processes (Fig. 7). The presence of phenocrysts and the amount of minerals formed by alteration are critical to the interpretation of the K–Ar geochronological data (Faure & Mensing 2005).

The phenocrysts are mainly plagioclase but subordinate amounts of clinopyroxene and olivine are also present. Plagioclase phenocrysts make up to 1 vol.% modally. Their size ranges from 0.1 to 5 mm. Plagioclase phenocrysts sometimes occur as glomeroporphyritic clusters (Fig. 5d). Most are normally zoned, their rims having compositions close to the composition of the smaller plagioclase laths that are the principal component

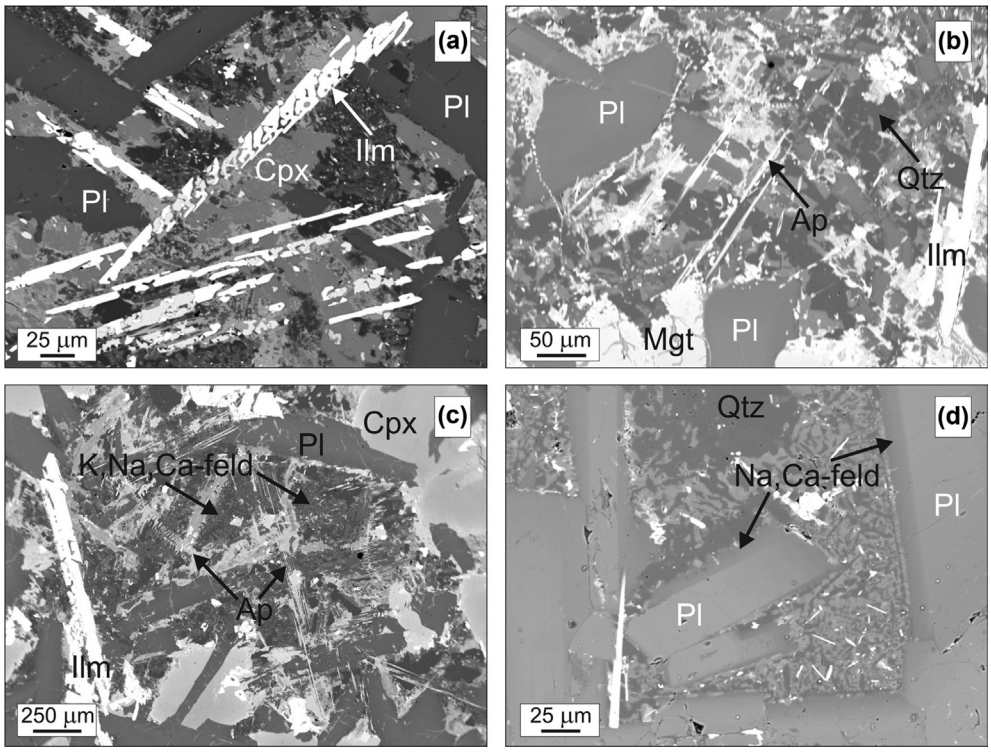

Fig. 6 Backscattered electron microscopy images of groundmass of dolerites in Svalbard. (a) Fine-grained dolerite consists of plagioclase, clinopyroxene and skeletal crystals of ilmenite; sample ES-10. (b) Intergrowths of feldspar with clinopyroxene and, inside, needle-like crystals of ilmenite and apatite and small amounts of quartz occur; sample ES-2. (c) Patch of fine-grained doleritic groundmass consists of Na–plagioclase, K–Na feldspar, skeletal apatite and Fe–Ti oxides; sample ES-6. (d) Labradorite grains showing thin, oligoclase-rich rims; sample ES-7. The fine-grained groundmass consists of clinopyroxene, plagioclase and subordinate quartz. Grains of apatite (Ap), clinopyroxene (Cpx), ilmenite (Ilm), alkali feldspar (K, Na, Ca–feld), magnetite (Mgt), plagioclase (Pl) and quartz (Qtz) are indicated.

of the dolerite. The absence of resorbed plagioclase phenocryts and plagioclase with a sieve texture is typical of Svalbard dolerites. The scarce clinopyroxene phenocrysts occur only in samples ES-2, GT-3 and CS-20. Olivine phenocrysts are generally altered to iddingsite.

The vast majority of dolerites, irrespective of texture, consist of the plagioclase laths forming a framework enclosed in, or overgrown by, clinopyroxene (Fig. 5a–c). The size of the plagioclase laths varies from submicroscopic to 0.6 mm, depending on the texture. Plagioclase laths form 45 to 50 vol.% of most samples. Olivine occurs only in some samples as euhedral microphenocrysts (Fig. 5e), with sizes comparable to the plagioclase laths. Most olivines are partly or completely altered to iddingsite (Fig. 7c).

Spaces between the plagioclase framework are filled by clinopyroxene aggregates with accessory amounts of Fe–Ti oxides. The clinopyroxene varies from submicroscopic to 0.4 mm in size. On backscattered electron microscopy images all clinopyroxene shows chemical zoning. Fe–Ti oxides in clinopyroxene occur as needles, skeletal and sometimes euhedral angular grains (Fig. 6a, c). The fine-grained groundmass is composed of plagioclase, clinopyroxene, alkali feldspar (compositions range from albite to sanidine, as deduced from analysis of mapping images that show distribution of elements), skeletal crystals of Fe–Ti oxides and apatite (Fig. 6b, c). Sulphides are represented by pyrite, chalcopyrite and bornite.

The secondary minerals (Fig. 7) in most samples are present in very small amounts; samples CS-24, CS-25, GT-2 and CS-19 are the most altered. Sericite, iddingsite, chlorite, unidentified clay minerals and Ca–Mg–Fe carbonates are secondary minerals. Traces of hematite and/or Fe hydroxides were also identified. The clinopyroxene in most samples is rather fresh, in contrast to olivine and some plagioclase, which shows more advanced alteration (Fig. 7a). In addition, in most dolerite samples that contain several volume percent of a brownish, cryptocrystalline mesostasis, the initial stages of replacement by clay minerals are observed. Secondary carbonates were identified in dolerites from the contacts with host rocks. Ca–Mg–Fe carbonates and brown clay minerals

Citation: *Polar Research* 2011, *30*, 7306, DOI: 10.3402/polar.v30i0.7306

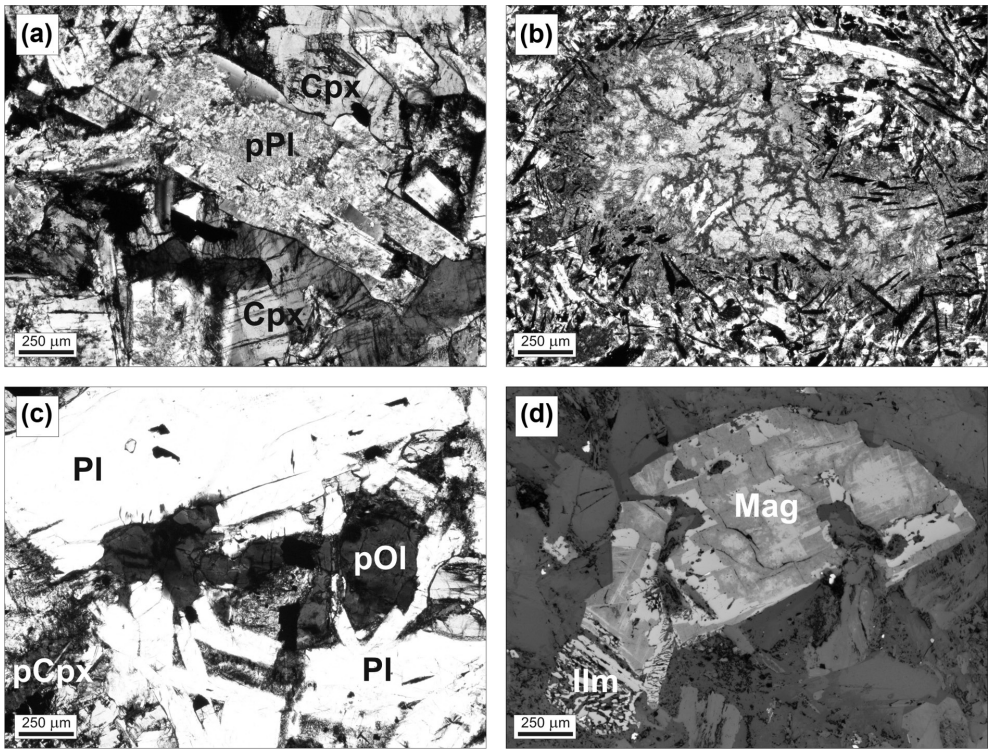

Fig. 7 Petrography of the alteration products of dolerites from Svalbard. (a) Sericitization of plagioclase; sample ES-8 (photographed with transmitted light, crossed nicols). (b) Amygdale composed of clay minerals; sample ES-1 (photographed with transmitted light, one nicol). (c) Iddingsite pseudomorph after olivine; sample ES-13 (photographed with transmitted light, one nicol). (d) Initial alteration of magnetite; sample CS-20 (photographed with reflected light, one nicol). Grains of clinopyroxene (Cpx), ilmenite (Ilm), magnetite (Mgt), plagioclase (Pl), iddingsite (pOl) and sericite (pPL) are indicated.

commonly fill vesicles (Fig. 7a) and form pseudomorphs after plagioclase and clinopyroxene.

Mineral chemistry

The chemical composition of plagioclase, alkali feldspars, clinopyroxene, olivine, Ti–magnetite, ilmenite and apatite were determined by electron probe micro-analysis. Representative microprobe analyses of plagioclase and clinopyroxene are presented in Table 2.

Feldspars

Electron probe micro-analyses revealed two distinct groups of feldspars, represented by plagioclase and alkali feldspars (Fig. 8a). The plagioclase, including rare phenocrysts, ranges from bytownite to andesine ($Or_{0.01–0.04}Ab_{0.28–0.99}An_{0.01–0.72}$). The highest An contents (>65% mol. An) were found in the cores of some normally zoned phenocrysts. Plagioclase from the fine-grained matrix is the richest in albite. Similar compositions were found in the rims of the plagioclase microphenocysts. The An content of this generation of plagioclase decreases to 43 mol.%. Alkali feldspars were identified in the fine-grained groundmass, their composition being in the range $Or_{53–63}Ab_{36–44}An_{1–3}$. Concentrations of SrO and BaO in the alkali feldspars are low, reaching 0.15 wt% (Table 2a).

Clinopyroxene

The clinopyroxene composition determined by electron probe micro-analysis corresponds to $En_{12.23–52.08}Wo_{10.88–43.73}Fs_{6.5–68.49}$. Most plot in the Mg–Ca–Fe quadrilateral in the augite field (Fig. 8b), backscattered electron microscopy images of the largest clinopyroxenes show a continuous Fe enrichment trend and the composition of the rims of the larger clinopyroxene grains is close to that of fine-grained clinopyroxenes from the groundmass. The Al_2O_3 contents range from 5.51 wt% in the cores to 0.26 wt% at the rims. The amounts of Na_2O and TiO_2 are up to 0.69 and 3.18 wt%, respectively (Table 2b).

Table 2 (a) Chemical composition of plagioclase from the Svalbard dolerites. (b) Chemical composition of clinopyroxene from the Svalbard dolerites.

(a)	CS-19	ES-1	ES-1	ES-2	ES-3a	GT-3	GT-3	BH-3C	BH-3C	BH-3B	BH-3B	ES-35	CS-19
SiO_2	56.69	52.52	50.06	54.20	53.73	52.42	57.47	54.38	53.72	68.01	68.01	66.05	66.45
Al_2O_3	26.72	29.53	31.49	28.76	28.90	29.56	26.41	27.86	28.44	20.27	20.27	19.01	19.36
FeO	0.75	0.64	0.63	0.68	0.56	0.69	0.74	0.74	0.86	0.42	0.42	0.12	0.14
MgO	0.02	0.18	0.13	0.17	0.18	0.19	0.07	0.13	0.17	0.08	0.08	0.00	0.02
CaO	9.21	13.08	14.31	11.30	12.20	13.03	9.17	11.29	11.89	0.24	0.24	0.40	0.35
Na_2O	5.65	3.85	3.06	4.37	4.46	3.88	5.80	4.49	4.30	10.92	10.92	4.32	4.31
K_2O	0.37	0.16	0.13	0.28	0.25	0.17	0.43	0.28	0.22	0.13	0.13	10.14	9.92
Total	99.41	99.96	99.81	99.77	100.27	99.93	100.09	99.17	99.59	100.06	100.06	100.04	100.55
Recalculated on the basis of eight oxygen atoms													
Si	2.564	2.388	2.290	2.455	2.431	2.386	2.582	2.479	2.445	2.969	2.969	2.987	2.984
Al	1.425	1.583	1.698	1.536	1.541	1.586	1.399	1.497	1.526	1.043	1.043	1.014	1.025
Fe^{2+}	0.028	0.024	0.024	0.026	0.021	0.026	0.028	0.028	0.033	0.015	0.015	0.004	0.005
Mg	0.001	0.012	0.009	0.011	0.012	0.013	0.005	0.009	0.011	0.005	0.005	0.000	0.001
Ca	0.446	0.637	0.701	0.548	0.591	0.635	0.441	0.552	0.580	0.011	0.011	0.019	0.017
Na	0.495	0.340	0.272	0.384	0.391	0.342	0.505	0.397	0.379	0.924	0.924	0.379	0.376
K	0.021	0.010	0.008	0.016	0.014	0.010	0.025	0.016	0.013	0.007	0.007	0.585	0.568
Total	4.982	4.995	5.001	4.977	5.001	4.997	4.984	4.979	4.987	4.975	4.975	4.989	4.976
Or[a]	0.02	0.01	0.01	0.02	0.01	0.01	0.03	0.02	0.01	0.01	0.00	0.61	0.59
Ab[b]	0.51	0.37	0.28	0.40	0.33	0.35	0.52	0.41	0.39	0.98	0.99	0.37	0.39
An[c]	0.46	0.62	0.72	0.58	0.66	0.64	0.45	0.57	0.60	0.01	0.01	0.02	0.02

(b)	CS-19	Bh-3a	Bh-3c	Bh-3a	ES-5	ES-12	ES-30	CS-23	ES-29	ES-34	GT-13	ES-29	ES-3a
SiO_2	50.78	49.40	45.52	49.56	49.60	49.27	51.43	47.58	51.02	50.45	50.55	48.69	50.73
Al_2O_3	2.02	0.62	3.16	0.55	1.99	2.26	3.07	2.69	3.34	2.69	3.83	3.85	1.06
Cr_2O_3	0.09	0.00	0.04	0.00	0.01	0.01	0.75	0.00	0.94	0.36	1.06	0.20	0.01
Fe_2O_3	1.44	0.56	4.67	0.96	2.42	2.25	1.47	0.00	1.53	1.75	1.46	2.37	0.00
FeO	10.37	30.65	18.46	30.97	13.19	12.78	5.34	31.74	4.87	8.43	3.90	8.76	19.90
MgO	14.93	11.07	10.74	11.45	15.12	13.72	17.02	4.55	16.74	15.81	16.73	14.47	14.20
MnO	0.26	0.68	0.33	0.62	0.37	0.30	0.16	0.40	0.11	0.20	0.08	0.22	0.38
TiO_2	1.13	0.46	1.59	0.40	1.31	1.53	0.61	0.11	0.61	1.14	0.50	1.85	0.67
CaO	18.23	6.31	13.25	5.66	14.81	16.76	19.46	8.86	19.80	18.30	20.44	18.70	11.63
Na_2O	0.25	0.07	0.19	0.07	0.20	0.27	0.27	0.48	0.30	0.23	0.20	0.25	0.13
Total	99.49	99.83	97.93	100.23	99.01	99.16	99.59	96.40	99.23	99.34	98.74	99.37	98.69
Recalculated on the basis of six oxygen atoms													
Si	1.91	1.966	1.816	1.964	1.891	1.888	1.895	1.987	1.886	1.887	1.874	1.835	1.963
Al.	0.089	0.029	0.148	0.026	0.089	0.102	0.133	0.132	0.145	0.118	0.168	0.171	0.048
Fe^{2+}	0.326	1.02	0.616	1.026	0.421	0.441	0.165	1.108	0.151	0.264	0.121	0.276	0.644
Fe^{3+}	0.041	0.017	0.14	0.029	0.069	0.034	0.041	0	0.042	0.049	0.041	0.067	0
Mg	0.837	0.656	0.638	0.676	0.859	0.784	0.935	0.283	0.922	0.882	0.924	0.813	0.819

Table 2 *Continued*

(b)	CS-19	Bh-3a	Bh-3c	Bh-3a	ES-5	ES-12	ES-30	CS-23	ES-29	ES-34	GT-13	ES-29	ES-3a
Mn	0.008	0.023	0.011	0.021	0.012	0.01	0.005	0.014	0.003	0.006	0.003	0.007	0.012
Ti	0.032	0.014	0.048	0.012	0.037	0.044	0.017	0.003	0.017	0.032	0.014	0.052	0.019
Cr	0.003	0	0.001	0	0	0	0.022	0	0.027	0.011	0.031	0.006	0
Ca	0.735	0.269	0.566	0.24	0.605	0.688	0.768	0.396	0.784	0.734	0.812	0.755	0.482
Na	0.018	0.006	0.015	0.005	0.015	0.02	0.02	0.039	0.021	0.017	0.014	0.018	0.009
Total	4	4	3.999	4	3.999	4.01	4	3.963	4	4	4	4	3.998
Wo[d]	38.72	13.77	29.9	12.23	31.43	35.97	41.14	21.01	42.23	39.04	43.73	40.95	24.72
En[e]	44.09	33.57	33.7	34.43	44.64	40.98	50.05	15.03	49.66	46.92	49.77	44.08	41.97
Fs[f]	17.19	52.66	36.41	53.34	23.93	23.05	8.82	63.96	8.11	14.04	6.5	14.97	33.31

[a]Orthoclase end-member.
[b]Albite end-member.
[c]Anorthite end-member.
[d]Wollastonite end-member.
[e]Enstatite end-member.
[f]Ferrosilite end-member.

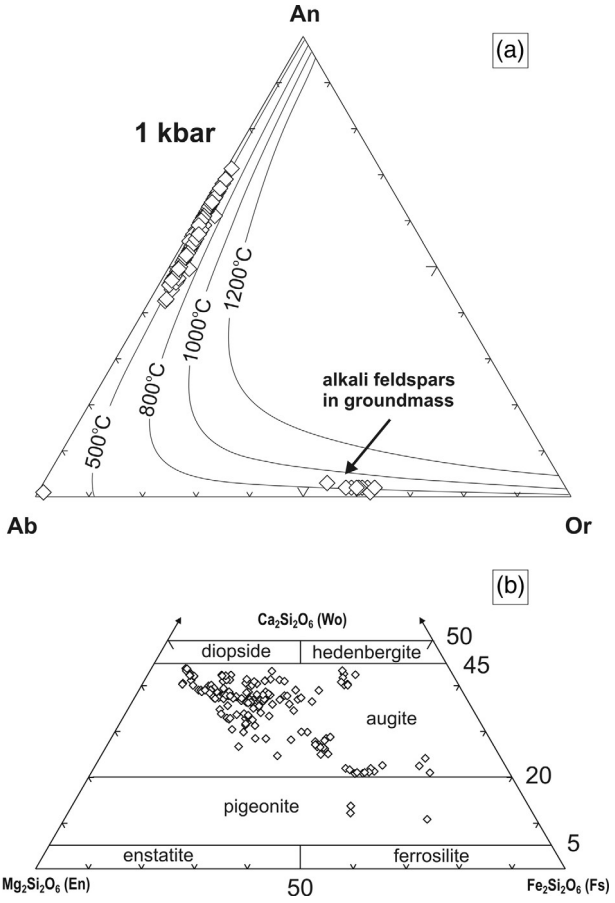

Fig. 8 Diagrams showing the chemical composition of feldspar and clinopyroxene in the Svalbard dolerites. (a) Composition of feldspars projected on triangular diagram of albite (Ab), anorthite (An) and orthoclase (Or) end-members. Tie lines on the diagram show the compositions of plagioclases and alkali feldspars that exist in equilibrium with each other at indicated temperatures and pressure close to 1 kbar. (b) Quadrilateral diagram (enstatite–ferrosilite–diopside–hedenbergite) of clinopyroxene from the Svalbard dolerites.

Olivine

The forsterite content of olivines from the Svalbard dolerites varies from 70.58 to 26.85 mol.%. Olivine phenocrysts are commonly more magnesian, while olivines crystallized together with plagioclase microphenocrysts are the richest in fayalite (>40 mol.%). The MnO content is high, up to 1 wt%, as opposed to CaO, which is commonly low and ranges from 0.29 to 0.19 wt%. NiO concentrations are below 0.26 wt%.

Fe–Ti oxides

Fe–Ti oxides occur as Ti–magnetite and ilmenite. Ti–magnetite shows a wide range of TiO_2 contents, varying

form 19.9 to 31.1 wt%. The ulvöspinel end-member is high in Ti–magnetite, which crystallized rapidly, especially in thin sills and also in borders of their thicker equivalents. Ti–magnetite with oxyexsolution intergrowths of ilmenite has distinctly lower contents of the ulvöspinel end-member (for details of oxyexsolution processes see Haggerty 1991). The ranges of Al_2O_3, MgO, MnO and NiO content in Ti–magnetite are 1.02–2.32, 0.01–0.43, 0.2–1.98 and 0.01–0.07 wt%, respectively. Two generations of ilmenite, crystallized from melt and oxyexsolution intergrowths, have similar composition. Hematite end-member in ilmenite is between 3.92 and 8.78 mol.%.

Apatite

Apatites in the dolerites have a rather constant composition, similar to that known in basaltic rocks. They are fluorapatite, with the concentration of F and SiO_2 varying from 3.77 to 4.92 wt% and from 0.33 to 4.57 wt%, respectively. The higher SiO_2 contents determined in apatite may reflect the occurrence of submicroscopic intergrowths of quartz and/or plagioclase in some skeletal apatite crystals. The SrO contents in apatite are below electron probe micro-analysis detection limits.

Whole rocks geochemistry

Major element data

The dolerites from Svalbard have SiO_2 contents ranging from 43.16 to 49.37 wt%, Al_2O_3 from 12.05 to 14.84 wt%, total iron recalculated as FeO_{tot} from 10.99 to 14.68 wt%, MgO from 2.67 to 7.67 wt% and CaO from 7.7 to 10.68 wt%. The TiO_2 and P_2O_5 contents are between 2.14 and 3.81 wt% and between 0.19 and 0.41 wt%, respectively. The Mg number (molar $Mg/[Mg+Fe^{2+}]$; $0.86*FeO_{(tot)}$ was used to calculate Fe^{2+}) falls in the range of 0.30–0.58. The more magnesian rocks with Mg number >50 have relative high Cr and Ni contents, reaching 200 and 108 ppm, respectively. The lowest Mg numbers, from 0.30 to 0.36, calculated in samples ES-1, ES-10, BH-3B and GT-13, correspond to the highest values of loss of ignition. The loss of ignition values of most of the dolerites are low, varying from 0.1 to 2.2 and indicate rather low or moderate alteration of the samples under study. Samples ES-1, ES-10, GT-13 and BH-3B are considerably altered, with loss of ignition values ranging from 7.6 to 9.4. The composition of representative samples is given in Table 3.

In the total alkali versus silica (TAS) classification of Le Bas et al. (1986), all the Svalbard dolerites are basalts (Fig. 9). CIPW norms, showing normative mineral compositions, were calculated for each dolerite sample and allowed their subdivision into two groups. On the basis of the degree of silica saturation, two dolerite types were recognized: (1) quartz tholeiite (quartz–hypersthene normative [Q+Hy]) and (2) olivine tholeiite (olivine–hypersthene normative [Ol+Hy]), as shown in Table 1. Dolerites of these groups are uniformly distributed between the eastern and central parts of Svalbard. On the alkaline (Na_2O+K_2O) – FeO_{total} – MgO diagram of Irvine & Baragar (1971) all dolerites define a clear tholeiitic trend.

Trace element data

The dolerites from Svalbard are characterized by relatively high La/Nb (1.07–1.51) and Zr/Y (4.08–5.45) values and low Ti/Yb (0.52–0.64) values. The Zr/Nb and La/Lu values range from 16.49 to 20.85 and from 25.89 to 34.23, respectively. The rocks show a distinct enrichment in light REE over heavy REE, clearly demonstrated by high $(La/Lu)_{cn}$ ratios that vary from 2.78 to 3.67 and there is a significant fractionation of middle REE over heavy REE, as shown by $(Tb/Yb)_{cn}$ ranging from 1.86 to 2.30. All dolerite patterns plotted in the REE diagram are parallel, showing no, or a negligible, Eu anomaly (Fig. 10a). The variation of Eu/Eu* ratio varying from 0.78 to 1.03 suggests that fractional crystallization of plagioclase in deeper parts of the magmatic plumbing system was moderate. This conclusion is confirmed by the limited amount of plagioclase phenocrysts observed in the dolerites. Spider diagrams of trace elements against their concentration in primitive mantle show clear convex-up patterns of all samples (Fig. 10b). All have characteristic P, Sr, Nb and Ba negative anomalies and three samples (ES-15, ES-17, ES-35) show significant Pb positive anomalies. Ba and Sr negative anomalies, together with moderate Eu anomaly, probably correspond to the fractionation of plagioclase during earlier stages of evolution of dolerite plumbing system. These processes were probably accompanied by simultaneous fractionation of apatite that is recorded by significant P anomaly (Fig. 10b). Crustal assimilation processes probably explain significant Nb negative anomalies, recognized in all Svalbard dolerites (Fig. 10b). The small positive Ti anomaly in all dolerites probably reflects a lack of fractionation of Fe–Ti oxides, while clear positive Y anomalies along with higher ratios of normalized $(HREE)_{cn}$ probably exclude garnet from the mantle source of the dolerite melts. The scattered amounts of Sr, Ba and K in a few samples record alteration processes, probably of feldspars.

Citation: *Polar Research* 2011, *30*, 7306, DOI: 10.3402/polar.v30i0.7306

Table 3 Concentrations of major (wt%) and trace elements (ppm) in selected samples of the Svalbard dolerites. Mg number (Mg#) is Mg/(Mg+Fe^{2+}); 0.86*$FeO_{(tot)}$ was used to calculate Fe^{2+}.

Sample	CS-23	CS-24	ES-11	ES-5	GT-13	GT-2	BH-3A	BH-3B
SiO_2	48.50	49.20	47.96	48.67	46.23	48.46	48.34	45.96
TiO_2	3.61	3.56	3.52	3.58	3.72	3.06	3.60	3.57
Al_2O_3	12.86	13.18	12.88	13.29	13.31	13.62	12.98	13.49
Cr_2O_3	0.01	0.01	0.02	0.01	0.01	0.03	0.01	0.02
Fe_2O_3	15.40	15.16	15.78	14.75	14.43	14.41	15.40	14.48
MnO	0.21	0.21	0.21	0.21	0.12	0.20	0.21	0.16
MgO	5.08	5.16	6.07	5.27	2.85	6.05	5.09	3.60
CaO	9.32	8.92	9.10	9.26	7.70	9.32	9.18	7.93
Na_2O	2.36	2.73	2.35	2.36	2.32	2.61	2.32	2.36
K_2O	0.64	0.93	0.68	0.75	0.37	0.82	0.69	0.22
P_2O_5	0.41	0.35	0.32	0.35	0.39	0.32	0.38	0.37
LOI[a]	1.50	0.50	1.00	1.40	8.30	1.00	1.70	7.60
Total	99.90	99.91	99.89	99.90	99.75	99.90	99.90	99.76
Mg#	0.43	0.44	0.47	0.45	0.31	0.49	0.43	0.36
Sr	285.9	349.3	300.00	308.30	393.6	350.4	293.2	365.5
Y	47.8	46.1	49.20	51.30	47.9	43.4	47.5	42.8
Zr	242.9	237	232.50	238.70	245	206	240.4	233.2
Hf	6.8	6.4	6.20	6.60	7.1	5.9	7.1	6.6
Nb	12.5	12	11.60	12.60	13.4	10.6	12	11.2
Ta	0.9	0.7	0.70	0.80	1	0.7	0.7	0.7
Ba	93.5	113.3	145.50	167.00	240.7	169.6	119.6	127.5
Pb	2	1.2	1.60	2.10	2.4	2.7	2.2	3.8
Th	3.3	2.4	2.80	3.10	3.4	3	4	2.9
U	0.7	0.8	0.70	0.80	1	0.8	1	1
La	16.5	16.4	16.10	17.50	18	15.6	17.3	16.7
Ce	44.9	44.2	45.50	47.90	46.9	40.4	46.4	44.3
Pr	7.02	6.96	6.53	6.82	7.45	6.07	7.08	6.91
Nd	31.3	31	32.20	32.90	32.3	30	32.5	29.6
Sm	7.87	7.33	7.74	7.95	8.21	7.01	8.07	7.61
Eu	2.65	2.66	2.43	2.55	2.63	2.43	2.67	2.42
Gd	9.56	9.53	8.71	9.07	9.26	8.26	9.54	8.56
Tb	1.82	1.83	1.62	1.66	1.82	1.64	1.88	1.72
Dy	8.43	8.54	7.91	8.21	9.19	8.03	8.68	8.3
Ho	1.67	1.65	1.49	1.55	1.68	1.54	1.73	1.59
Er	4.59	4.38	4.10	4.33	4.83	4.2	4.85	4.4
Tm	0.68	0.66	0.63	0.64	0.7	0.59	0.68	0.63
Yb	3.81	3.61	3.57	3.82	3.84	3.5	3.87	3.6
Lu	0.59	0.53	0.51	0.53	0.62	0.55	0.54	0.53
$REE^{b}_{(tot)}$	141.39	139.28	139.04	145.43	147.43	129.82	145.79	136.87

[a]Loss of ignition value.
[b]Rare earth element.

Geotectonic setting of dolerites from Svalbard

The concentrations of major and trace elements were used to elucidate the tectonic setting of the Svalbard dolerites. In the major-element plot of Pearce et al. (1977), the data are generally scattered close to the border between continental basalts and ocean island basalts (Fig. 11a). An affinity to within-plate basalts is suggested by projection of the data into the Zr–Ti–Y diagrams of Pearce & Norry (1979; not shown) and Pearce & Cann (1973; Fig. 11b), respectively. The within-plate nature of the rocks is verified using the diagram of Meschede (1986; Fig. 11c). On the Ti versus *V* diagram of Shervais (1982; not shown), all dolerite samples plot slightly above a line defined by the Ti/*V* = 50 ratio and group in a narrow field located between the fields of continental flood basalt and ocean–island/alkali basalt. The diagram proposed by Cabanis & Lecolle (1989) shows geochemical characteristics typical of

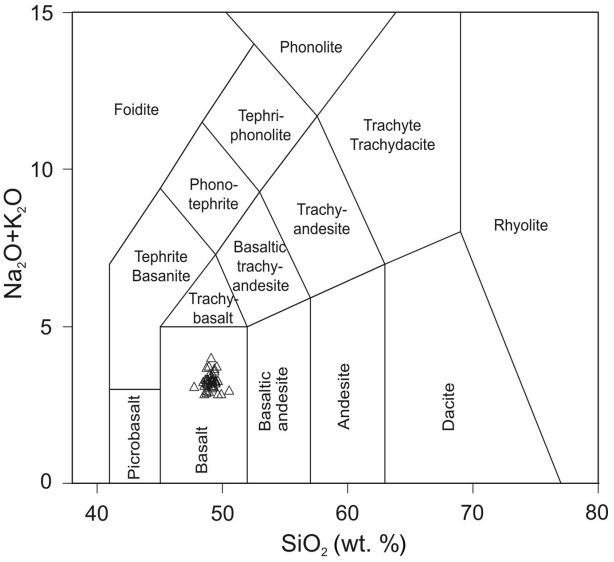

Fig. 9 Systematic position of Svalbard dolerites on the total alkali versus silica (TAS) classification diagram (LeBas et al. 1986).

continental basalts for all the material analysed in this study (Fig. 11d).

Geochronology of dolerites from Svalbard

Thirty-nine samples were selected for geochronological study by the K–Ar method (Table 4). The samples were taken from outcrops scattered in the major eastern Svalbard dolerite belt and from the central Spitsbergen dolerite centre, mainly from the Isfiorden area (Fig. 2). The results are in the time span from 125.5 ± 3.6 to 78.3 ± 2.6 Mya. One sample (ES-10) is significantly older (257 ± 7.3 My). Additionally, dating of one dolerite sample (WS-0) from the western Spitsbergen thrust-and-fold belt in the Bellsund area (Birkenmajer 1972; Harland & Horsfield 1974) yielded an age of 118.7 ± 6.8 My. The great analytical error is the consequence of the high Ar_{atm} contamination, resulting from alteration of the sample.

Our data suggest that the continuous intraplate dolerite magmatism in Svalbard displays four distinct maxima of intensive activity, calculated using statistical processing of all geochronological data available (Fig. 12). Sample ES-10 is highly altered and its K–Ar age was excluded from the calculation. The peaks of intensive activity are identified as having occurred at 115.3, 100.8, 91.3 and 78.5 Mya, all with $\pm 2\sigma$ varying from 3.2 to 7.3 My (Fig. 12). Some dolerites from eastern Svalbard might represent an additional, slightly older, maximum at 123.6 ± 6.1 Mya. Comparing the geochronological results for dolerites from central and eastern parts of Svalbard revealed that the eastern Svalbard dolerites lack the 91.3 Mya peak of magmatic activity. However, in both areas magmatic activity was terminated ca. 80 Mya (Fig. 12). Interesting results were obtained from three age determinations (GT-1–3) across one of the thickest dolerite sills in central Spitsbergen (Fig. 3). The sill at Grønsteinfjellet, up to 40 m thick, has yielded similar K–Ar dates at its margins (115.8 and 117.3 Mya) but a much younger date in its central part (78.6 Mya). This thick sill may represent a group of composite sills that consist of stacking sills developed during different episodes of intrusion of doleritic melts (e.g., Menand 2008). Unfortunately, we do not have field evidence of chilled margins that bordered the youngest dyke in the central part of the composite sill. The other possible explanations might involve either contamination of the dolerite by host rocks or hydrothermal alteration of the central, more coarse-grained, part of the sill. Anomalously old ages in border parts of mafic dykes may result from excess argon that was easily incorporated from the wet host rocks during rapid crystallization of the mafic rocks (Dalrymple & Moore 1968; Kelley 2002). This process is likely to explain different ages of the samples CS-19 and CS-20 taken from outer parts of the same sill at Diabasodden (Fig. 3a).

Discussion and conclusions

Dolerites from Svalbard constitute a monotonous series of mafic rocks from the point of their petrography, mineralogy and chemistry. They consist of plagioclase, clinopyroxene, alkali feldspar, Fe–Ti oxides and the accessory minerals, including olivine, apatite, quartz, pyrite, chalcopyrite and bornite. The dolerites are uniformly within-plate tholeiites. Trace-element geochemistry reflects their continental intra-plate setting. Rocks that have similar characteristics are known from several other localities in the Arctic (Fig. 1). All these occurrences were defined by Tarduno (1998) and Maher (2001) as components of HALIP, which formed during the opening of the Arctic Ocean.

Mafic rocks, including basic lava flows and dolerite sills and dykes, similar to those described here, are known from Kong Karls Land in easternmost Svalbard and the archipelago of Franz Josef Land (Smith et al. 1976; Bailey & Rasmussen 1997; Dibner 1998; Ntaflos & Richter 2003). Based on field observations, six events of intensive volcanic activity were recognized (Smith et al. 1976), resulting in numerous sills and lava flows associated with pyroclastic rocks. Products of this magmatism were also

Citation: *Polar Research* 2011, *30*, 7306, DOI: 10.3402/polar.v30i0.7306

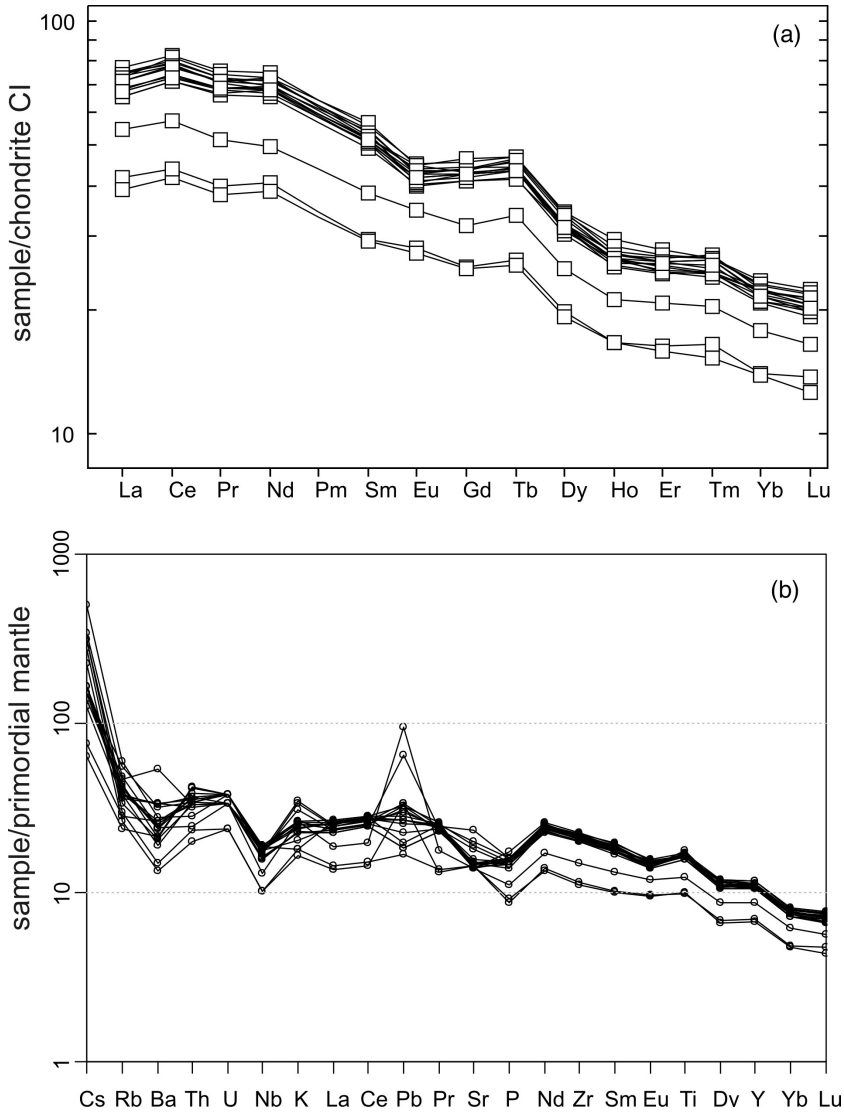

Fig. 10 (a) Chondrite normalized rare earth element patterns and (b) primitive mantle normalized trace element diagram. Normalization factors are from Sun & McDonough (1989).

dredged from surrounding submarine areas (Grogan et al. 2000). These rocks record the initial stage of rifting of the margin of the Barents Shelf and adjacent areas that took place during the Cretaceous. Geochemistry of studied dolerites from Svalbard is similar to tholeiitic basalts from Franz Josef Land (for details see Ntaflos & Richter 2003). However, Nb–Ta contents suggest more extensive crustal contamination of doleritic melts from Svalbard. Mafic intra-plate magmatism that may be correlated with the HALIP was also described from De Long Island (Silantyev et al. 2004; Fedorov et al. 2005). The rocks are alkali basalts, with K–Ar ages varying from 124 to 106 My.

Magmatic rocks related to the opening of the Arctic Ocean are widespread in the Canadian Arctic (Estrada & Henjes-Kunst 2004). Their composition is similar to the Svalbard dolerites and geochemical parameters indicate their connection to initial rifting related to the opening of the Canada Basin (Bailey & Rasmussen 1997). Most of the rocks occur as dykes and sills (Buchan & Ernst 2006), although lavas and thick pyroclastic deposits are also known (Embry & Osadetz 1988). Some parts of these volcanics, for example, those occurring at the Hansen Point in Ellesmere Island (Estrada & Henjes-Kunst 2004), have bimodal and alkaline characteristics that unequivocally show their connection with the development of a

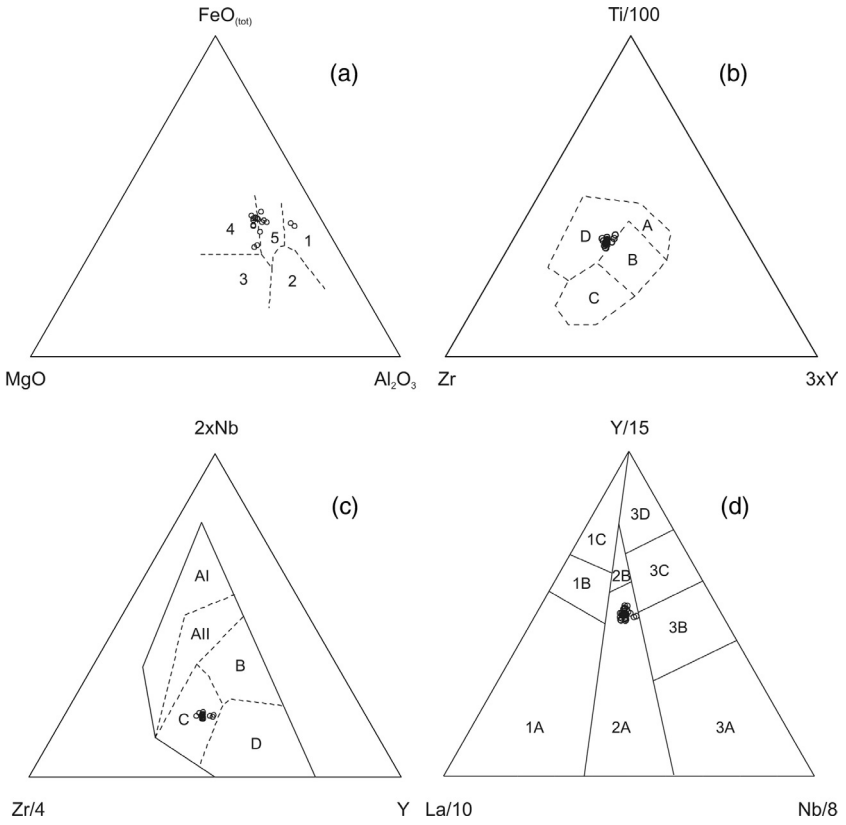

Fig. 11 Diagrams used for discriminating the tectonic environment of the Svalbard dolerites. (a) The MgO–FeO–Al_2O_3 diagram of Pearce et al. (1977) with fields for: spreading island centre (1), orogenic (2), ocean ridge and floor (3), ocean island (4) and continental (5) basalts. (b) The Zr–Ti–Y diagram of Pearce & Cann (1973) with fields for: island-arc tholeiites (A), mid-ocean ridge basalts, calc-alkali basalts and island-arc tholeiites (B), calc-alkali basalts (C) and within-plate basalts (D). (c) The Zr–Nb–Y diagram of Meschede (1986) with fields for: within-plate alkali basalts (AI), within-plate alkali basalts and within-plate tholeiites (AII), E-type mid-ocean ridge basalts (B), within-plate tholeiites and volcanic arc basalts (C) and N-type mid-ocean ridge basalts and volcanic arc basalts (D). (d) The La–Y–Nb diagram of Cabanis & Lecolle (1989) with fields for: calc-alkali basalts (1A), volcanic-arc tholeiites (1C), a field intermediate between 1A and 1C (1B), continental basalts (2A), back-arc basin basalts (2B), alkali basalts from intercontinental rift (3A), enriched-type mid-ocean ridge basalts (3B), weakly enriched E-type mid-ocean ridge basalts (3C) and N-type mid-ocean ridge basalts (3D).

continental rift system. The rocks include alkali basalts, trachyandesites, rhyodacites and rhyolites (Estrada et al. 2006).

Basic rocks similar to those occurring in Svalbard were also described from Kap Washington in Greenland (Brown et al. 1987; Kontak et al. 2001). These rocks have the characteristics of within-plate alkaline basalts. Mafic rocks occur together with rhyolites and comendites, suggesting the bimodal nature of the magmatic suite from Kap Washington.

HALIP also includes plutonic rocks. Among the best known is the Wootton Instrusive Complex in the northern part of Ellesmere Island (Estrada et al. 2006), where gabbro and minor amounts of granite have been recognized. The U–Pb ages of zircons separated from these plutonic rocks are 93 and 92 My (Trettin & Parrish 1987). Early Cretaceous granites are known from the Bol'shoi Lyakhov Island in the New Siberian Islands. Their radiometric ages, which Kos'ko & Trufanov (2002) obtained through different methods, are: 118.69 ± 0.42 and 120 ± 1.7 My (zircon, U–Pb), from 118 ± 6 to 122 ± 7 My (biotite, K–Ar) and from 112 ± 5 to 114 ± 6 My (microcline, K–Ar). Basic and acidic dykes have also been reported from this island.

Our new K–Ar results from the Svalbard dolerites are in very good agreement with the dates of 110 ± 5 and 100 ± 4 Mya published by Vincenz et al. (1981, 1984) and also partly with the first radiometric data (110–149 Mya), presented by Gayer et al. (1966). A preliminary dating of basalts and dolerites from Kong Karls Land using the Ar–Ar method (Grogan et al. 2000) has yielded 130–100 Mya for these rocks, which is in good agreement with the results presented in this study. An ongoing study of dolerites from the Bellsund area shows more dates in the

Citation: *Polar Research* 2011, *30*, 7306, DOI: 10.3402/polar.v30i0.7306

Table 4 Results of K–Ar dating of dolerites from different areas of Svalbard: the eastern Svalbard dolerite belt (sample numbers beginning with ES), the central Spitsbergen dolerite centre (CS as well as samples GT1–3, GT-13 and BH-3C), eastern Spitsbergen (S) and western Spitsbergen (WS). The number in the second column corresponds to the laboratory log number at the Institute of Nuclear Research of the Hungarian Academy of Sciences (Debrecen, Hungary). For sample details see Table 1.

	No. of K/Ar	Sample no.	Locality	*K* (%)	$^{40}Ar_{rad}$ (ccSTP/g)	$^{40}Ar_{rad}$ (%)	K/Ar age (My)
1	6833	ES-1	Bjørnbukta, Edgeøya	0.51	2.083×10^{-6}	50.6	102.1 ± 3.6
2	6834	ES-2	Andréetangen (I), Edgeøya	0.62	2.808×10^{-6}	77.88	112.9 ± 3.5
3	6835	ES-3	Pongtongen (I), Edgeøya	0.65	2.851×10^{-6}	80.8	109.4 ± 3.4
4	6837	ES-4	Pongtongen (II), Edgeøya	0.67	3.137×10^{-6}	72.8	116.6 ± 3.7
5	6839	ES-5	Zieglerøya, Tjuvfjorden	0.62	2.856×10^{-6}	70.8	114.8 ± 3.7
6	6840	ES-6	Andréetangen (II), Edgeøya	0.65	2.567×10^{-6}	72.7	98.8 ± 3.1
7	6841	ES-7	Habenichtbukta, Edgeøya	0.55	2.481×10^{-6}	68.1	125.5 ± 3.6
8	6842	ES-8	Dolerittneset (I), Edgeøya	0.89	3.579×10^{-6}	75.3	100.6 ± 3.2
9	6843	ES-9	Dolerittneset (II), Edgeøya	0.63	2.828×10^{-6}	76.4	111.9 ± 3.5
10	6843	ES-10	Leehovden, Edgeøya	0.55	5.905×10^{-6}	80.1	257.0 ± 7.3
11	6844	ES-11	Talaveraflya, Barentsøya	0.56	2.604×10^{-6}	68.0	115.8 ± 3.7
12	6845	ES-12	Sundneset, Barentsøya	0.88	3.644×10^{-6}	80.0	103.5 ± 3.0
13	6846	ES-13	Jakimovičøyane, Storfjorden	0.71	2.826×10^{-6}	72.2	99.6 ± 3.2
14	6847	ES-14	Ekrollhamna, Edgeøya	0.89	2.769×10^{-6}	59.8	78.3 ± 2.6
15	6848	ES-15	Heimland, Barentsøya	0.67	3.226×10^{-6}	74.8	119.8 ± 3.8
16	6849	ES-16	Ormholet (W), Barentsøya	0.41	1.867×10^{-6}	62.2	113.5 ± 3.8
17	6850	ES-17	Ormholet (E), Barentsøya	0.40	1.767×10^{-6}	51.8	110.2 ± 3.9
18	7172	CS-18	Gipshukodden, Spitsbergen	0.715	3.156×10^{-6}	60.7	110.1 ± 3.6
19	7173	CS-19	Diabasodden (W), Spitsbergen	0.847	2.715×10^{-6}	42.9	80.6 ± 3.1
20	7174	CS-20	Diabasodden (E), Spitsbergen	0.558	2.067×10^{-6}	46.3	92.9 ± 3.5
21	7175	CS-21	Hatten, Spitsbergen	0.523	2.197×10^{-6}	59.7	104.9 ± 3.5
22	7176	CS-22	Blomesletta, Spitsbergen	0.878	3.289×10^{-6}	50.7	93.9 ± 3.3
23	7177	CS-23	Kapp Thordsen (W), Spitsbergen	0.518	2.471×10^{-6}	55.0	118.7 ± 4.1
24	7178	CS-24	Gåsøyane, Spitsbergen	0.711	2.718×10^{-6}	53.8	95.8 ± 3.3
25	7179	CS-25	Gåsodden, Spitsbergen	0.940	3.338×10^{-6}	58.7	89.1 ± 3.0
26	7180	CS-26	Kapp Thordsen (E), Spitsbergen	0.772	3.678×10^{-6}	59.3	118.6 ± 3.9
27	7181	WS-0	Akseløya, Spitsbergen	0.442	1.865×10^{-6}	25.0	118.7 ± 6.8
28	7182	GT-1	Grønsteinfjellet, Spitsbergen (upper part)	0.643	2.989×10^{-6}	65.8	115.8 ± 3.7
29	7183	GT-2	Grønsteinfjellet, Spitsbergen (middle part)	0.718	2.241×10^{-6}	50.3	78.6 ± 2.8
30	7184	GT-3	Grønsteinfjellet, Spitsbergen (lower part)	0.605	2.851×10^{-6}	59.2	117.3 ± 3.9
31	7185	GT-13	Grønsteinfjellet, Spitsbergen (thin dyke)	0.294	1.302×10^{-6}	26.1	110.5 ± 6.1
32	7186	BH-3C	Botneheia (E), Spitsbergen	0.631	3.033×10^{-6}	61.0	119.6 ± 3.9
33	7187	ES-29	Sparreneset, Nordaustlandet	0.474	2.130×10^{-6}	62.9	112.1 ± 3.7
34	7188	ES-30	Kalkstranda, Nordaustlandet	0.475	1.887×10^{-6}	66.0	99.4 ± 3.2
35	7189	ES-31	Halvmåneøya, SE of Edgeøya	0.729	3.376×10^{-6}	55.1	115.4 ± 3.9
36	7190	S-32	Øgledalen, Spitsbergen	0.491	2.323×10^{-6}	80.4	117.8 ± 3.6
37	7191	ES-33	Isormen, Barentsøya	0.536	2.284×10^{-6}	75.0	106.4 ± 3.3
38	7192	ES-34	Wahlbergøya, Hinlopenstretet	0.630	2.727×10^{-6}	61.1	108.1 ± 3.6
39	7193	ES-35	Wilhelmøya, Hinlopenstretet	0.748	3.743×10^{-6}	68.1	124.3 ± 4.0

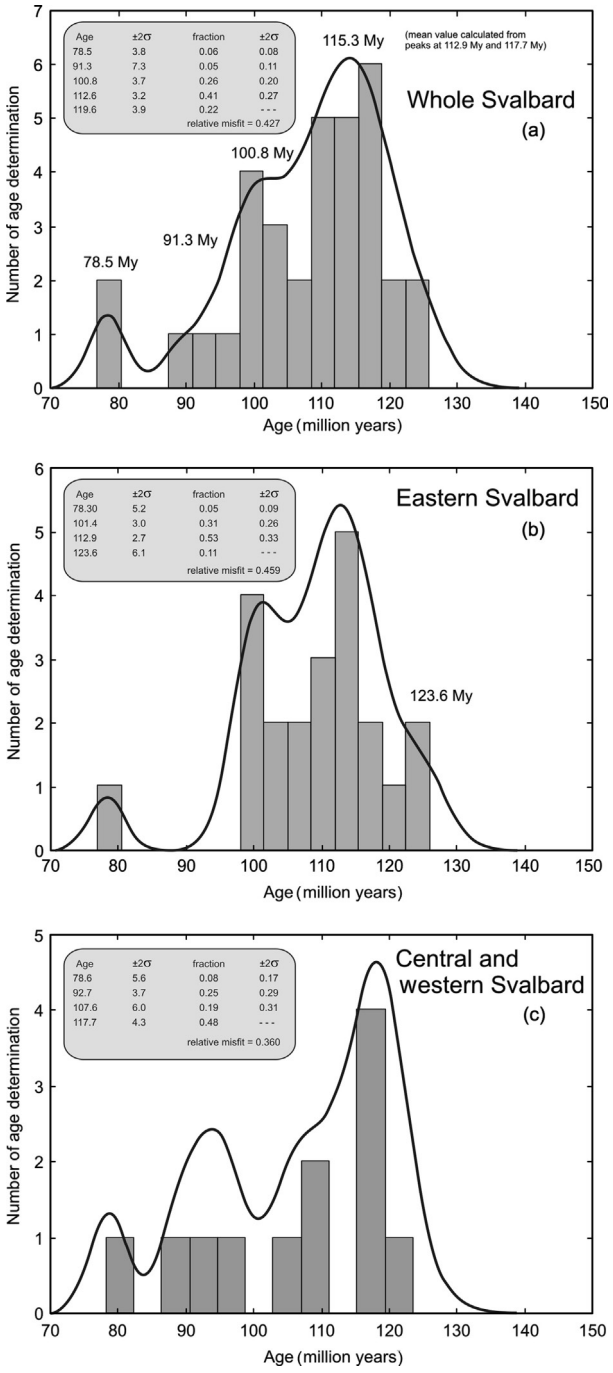

Fig. 12 Histograms and cumulative Gaussian plots showing results of K–Ar dating investigations of the dolerites (a) across Svalbard, (b) in eastern Svalbard and (c) in central and western Svalbard. Deconvolution of multiple age components was done using the Sambridge & Compston (1994) algorithm. Calculations were performed using Isoplot 3.7 software (Ludwig 2008).

range between 87.8 ± 6.2 and 109.4 ± 5.2 Mya (Birkenmajer et al. 2010). Comparison with the largest set of geochronological data already published for the Svalbard dolerites (Burov et al. 1977) clearly indicates a shorter duration of magmatism in our results (ca. 47 My) than the ca. 105 My determined by these authors. They inferred that the development of magmatic activity occurred in two major episodes, with age maxima at 144 ± 5 and 105 ± 5 My.

Dolerites from Svalbard are continental within-plate tholeiites that constitute part of HALIP and are related to the opening of the Arctic Ocean (Maher 2001). Rifting processes took place between 148 and 70 Mya (Fig. 13), as revealed by the geochronology of magmatic rocks identified as belonging to HALIP. These ages are also confirmed by dating the seafloor formation in the Amerasia Basin by means of different methods (for details see Sweeney 1985). Results of seismic and magnetic, as well as heat flow, measurements show that most of the seafloor originated between 118 and 83 Mya (Sweeney 1985).

A shorter time period of this activity documented by our new results is consistent with geochronological data obtained from different fragments of HALIP (Fig. 13), which originated from 131 to 80 Mya. The marked peaks of magmatic activity (Fig. 12) correlate well with stages of magmatic activity recognized in the Canadian Arctic (Embry & Osadetz 1988; Estrada & Henjes-Kunst 2004).

The magmatic rocks occurring in the Alpha and Mendeleyev ridges are related to HALIP magmatism (Maher 2001). Knowledge of the geology of these parts of the Amerasia Basin is very limited. The Alpha Ridge has been interpreted as a hot spot track, an oceanic plateau and a spreading centre (e.g., Jackson et al. 1986; Maher 2001; Silantyev et al. 2004) and was probably formed during or after the opening of the Canada Basin (Jokat 2003). According to Mukasa et al. (2009), preliminary petrological data obtained from two dredged samples of low-alkaline basalt from the Alpha Ridge have intraplate characteristics and are geochemically similar to mafic rocks from Ellesmere Island and Greenland. A Late Cretaceous Ar–Ar age of 82 ± 1 My has recently been obtained in a basalt sample from the Alpha Ridge (Jokat 2003). A Late Cretaceous age of highly altered basalt sample dredged from the Alpha Ridge is also mentioned by Brumley et al. (2008).

Similarities in age and geochemistry of mafic rocks from Svalbard, the Canadian Arctic Archipelago and Alpha Ridge may reflect contemporaneous tectonic processes that took place during the evolution of the Alpha Ridge. This may also correspond to pulses of magmatic activity responsible for development of the Alpha Ridge and the surrounding deep oceanic basins. In the evolution of the Amerasia Basin, these stages are defined as follows (Sweeney 1985): (1) ca. 130–120 Mya:

Citation: *Polar Research* 2011, *30*, 7306, DOI: 10.3402/polar.v30i0.7306

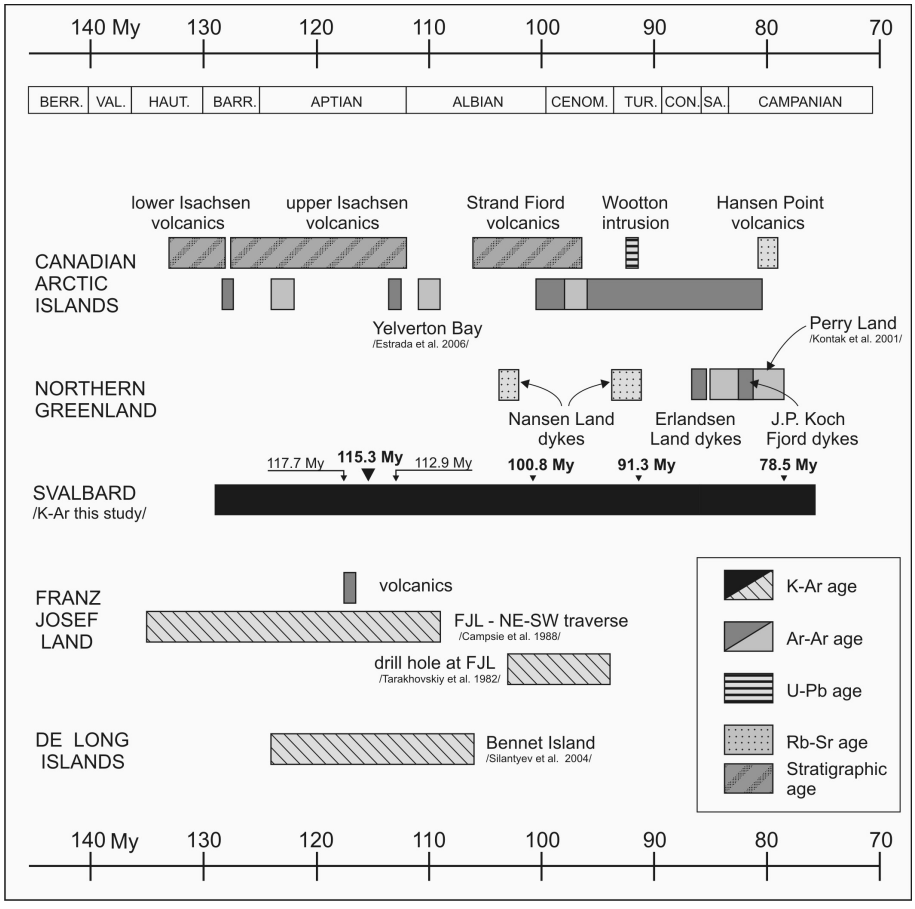

Fig. 13 Compilation of ages of mafic rocks from different parts of the High-Arctic Large Igneous Province including results of this study (marked with analytical errors). The scheme of the figure and geochronological data for the Canadian Arctic and Greenland have been taken from Buchan & Ernst (2006) and references therein. The compilation uses data from Tarakhovskiy et al. (1982), Campsie et al. (1988), Estrada et al. (2006), Kontak et al. (2001) and Silantyev et al. (2004). The black triangles mark calculated peaks of magmatic activity. The stratigraphic timescale is taken from Ogg et al. (2008).

initial magmatic processes related to activity of the mantle plume located in the southern part of Alpha Ridge; (2) ca. 120 – 110 Mya: early rifting, more intensive magmatic activity in all parts of HALIP, breakup of the continental crust and formation of the initial rift; (3) ca. 110–90 Mya: magmatic activity related to spreading processes along the Alpha Ridge that led to the development of the initial oceanic crust; (4) ca. 90–78 Mya: continuation of spreading along the Alpha Ridge, termination of HALIP-related magmatic activity.

The age of sample ES-10 close to 257 ± 7.4 My differs significantly from most analysed samples. However, this age is reported from HALIP by several researchers (e.g., Burov et al. 1977). The petrographical analysis of this sample revealed only moderate alteration processes, indicating that the variation in K probably controls the age of the sample. This age could likely be interpreted as a result of contamination of doleritic melts by older crustal material. The effects of excess and/or inherited argon may also explain the significantly older age of this dolerite sample.

Acknowledgements

Fieldwork in Svalbard was supported by the Polish Ministry of Science and Higher Education (grant nos. N 307 069 32/4103 and IPY/279/2006) and made possible by the scientific cruises of the SBS *Horyzont II*. The field assistance of Przemyslaw Karcz, Marcin Klisz and Stanislaw Mazur during the summer seasons of 2005 and 2007 is gratefully acknowledged. Special thanks are due to the Norwegian Petroleum Directorate for inviting KPK to join its expeditions to eastern Svalbard in August 2007 and August 2009 on board the MS *Kongsøy*. Atle Mørk, of SINTEF Petroleum Research, is thanked for dolerite samples from Isormen, Wilhelmøya and Wahlbergøya. The authors are grateful to Professors Krzysztof Birkenmajer and Raymond Macdonald for valuable suggestions

and for critical reviews of an earlier draft of the article. We would like to thank Richard Ernst, Solveig Estrada and Friedhelm Henjes-Kunst for their careful reviews of this article and their constructive comments. The authors are also grateful to Piotr Dzierzanowski and Lidia Jezak for their help with the electron probe micro-analyses, to Bozena Lacka for her help during preparation of the samples for geochemical and geochronological analyses and to Ewa Deput for preparation of the thin sections.

References

Bailey J.C. & Rasmussen M.H. 1997. Petrochemistry of Jurassic and Cretaceous tholeiites from Kong Karls Land, Svalbard, and their relation to Mesozoic magmatism in the Arctic. *Polar Research 16*, 37–62.

Balogh K. 1985. K/Ar dating of Neogene activity in Hungary: experimental technique, experiences and methods of chronologic studies. *ATOMKI Reports D/1*, 277–288.

Birkenmajer K. 1972. Tertiary history of Spitsbergen and continental drift. *Acta Geologica Polonica 22*, 194–218.

Birkenmajer K. 1986. Tertiary tectonic deformation of Lower Cretaceous dykes in a Precambrian terrane, south-west Spitsbergen. *Studia Geologica Polonica 89*, 31–44.

Birkenmajer K., Krajewski K.P., Lorenc M.W. & Pecskay Z. 2010. K–Ar dating of some dolerite intrusions at Bellsund, Spitsbergen, Svalbard. *Polish Polar Research 31*, 3–16.

Birkenmajer K. & Morawski T. 1960. Dolerite intrusions of Wedel-Jarlsberg Land, Vestspitsbergen. *Studia Geologica Polonica 4*, 103–123.

Brown P.E., Parsons I. & Becker S.M. 1987. Peralkaline volcanicity in the Arctic Basin—the Kap Washington volcanics, petrology and palaeotectonics. *Journal of Geological Society 144*, 707–715.

Brumley K., Mayer L.A., Miller E.L. & Coakley B. 2008. Dredged rock samples from the Alpha Ridge, Arctic Ocean: implications for the tectonic history and origin of the Amerasian Basin. *Eos, Transactions of the American Geophysical Union 89,* Fall Meeting Supplement, abstract T43B-2013.

Bryan S.E. & Ernst R.E. 2007. Revised definition of Large Igneous Provinces (LIPs). *Earth-Science Reviews 86*, 175–202.

Buchan K.L. & Ernst R. 2006. Giant dyke swarms and the reconstruction of the Canadian Arctic islands, Greenland, Svalbard and Franz Josef Land. In E. Hanski et al. (eds.): *Dyke swarms: time markers of crustal evolution*. Pp. 27–37. London: Taylor & Francis.

Burov Y.P., Krasil'schchikov A.A., Firsov D.V. & Klubov B.A. 1977. The age of Spitsbergen dolerites. *Norsk Polarinstitutt Årbok 1975*, 101–108.

Cabanis B. & Lecolle M. 1989. Le diagramme La/10-Y/15-Nb/8: un outil pour la discrimination des series volcaniques et la mise en evidence des processus de mélange et/ou de contamination crustale. (The La/10-Y/15-Nb/8 diagram: a tool for distinguishing volcanic series and discovering crustal mixing and/or contamination.) *Comptes Rendus de l'Academie des Sciences, Serie II, Sciences de la Terre 309*, 2023–2029.

Campsie J., Rasmussen M.H., Hansen N., Liebe C.J., Laursen J., Brochwicz-Lewinski W. & Johnson L. 1988. K–Ar ages of basaltic rocks collected during a traverse of Franz Josef Land Archipelago (1895–1896). *Polar Research 6*, 173–177.

Dallmann W.K. (ed.) 1999. *Lithostratigraphic lexicon of Svalbard. Upper Palaeozoic to Quaternary bedrock. Review and recommendations for nomenclature use*. Tromsø: Norwegian Polar Institute.

Dallmann W.K., Birkenmajer K., Hjelle A., Mørk A., Ohta Y., Salvigsen O. & Andresen A. 1993. *Description of geological map of Svalbard 1:100000, sheet C13G Sorkapp. Norsk Polarinstitutt Temakart 17*. Oslo: Norwegian Polar Institute.

Dallmann W.K., Ohta Y., Elvevold S. & Blomeier D. (eds.) 2002. *Bedrock map of Svalbard and Jan Mayen. Norsk Polarinstitutt Temakart* 33. Tromsø: Norwegian Polar Institute.

Dalrymple D.G. & Moore J.G. 1968. Argon 40: excess in submarine pillow basalts from Kilauea Volcano, Hawaii. *Science 161*, 1132–1135.

Dalrymple G.B. & Lanphere M.A. 1969. *Potassium–argon dating: principles, techniques, and applications to geochronology*. San Francisco: W.H. Freeman Co.

Dibner V.D. 1998. *Geology of Franz Josef Land. Norsk Polarinstitutt Meddelelser 146*. Oslo: Norwegian Polar Institute.

Embry A.F. & Osadetz K.G. 1988. Stratigraphy and tectonic significance of Cretaceous volcanism in the Queen Elizabeth Islands, Canadian Arctic Archipelago. *Canadian Journal of Earth Sciences 25*, 1209–1219.

Ernst R.E., Buchan K.L. & Campbell I.H. 2005. Frontiers in Large Igneous Province research. *Lithos 79*, 271–297.

Estrada S. & Henjes-Kunst F. 2004. Volcanism in the Canadian High Arctic related to the opening of the Arctic Ocean. *Zeitschrift der Deutschen Geologischen Gesellschaft 154*, 579–603.

Estrada S., Piepjohn K., Henjes-Kunst F. & von Gossen W. 2006. Geology, magmatism and structural evolution of the Yelverton Bay Area, northern Ellesmere Island, Arctic Canada. *Polarforschung 73*, 59–75.

Faure G. & Mensing T.M. 2005. The K–Ar method. In G. Faure & T.M. Mensing (eds.): *Isotopes. Principles and applications*. Pp. 113–143. Hoboken, NJ: John Wiley & Sons.

Fedorov P.I., Flerov G.B. & Golobin D.I. 2005. Novye dannye o vozraste i sostave vulkaničeskih porod ostrova Benetta (Vostočnaja Arktika). (New data on the age and composition of volcanic rocks on Bennett Island [East Arctic]. *Doklady Akademii Nauk 400*, 666–670.

Gayer R.A., Gee D.C., Harland W.B., Miller J.A., Spall H.R., Wallis R.W. & Winsnes T.S. 1966. *Radiometric age determination on rocks from Spitsbergen. Norsk Polarinstitutt Skrifter 137*. Oslo: Norwegian Polar Institute.

Grogan P., Nyberg K., Fotland B., Myklebust R., Dahlgren S. & Riis F. 2000. Cretaceous magmatism south and east of Svalbard: evidence from seismic reflection and magnetic data. *Polarforschung 68*, 25–34.

Haggerty S.E. 1991. Oxide textures—a mini-atlas. *Reviews in Mineralogy 25*, 129–219.

Harland W.B. 1997. *The Geology of Svalbard. Geological Society Memoir 17*. London: The Geological Society.

Harland W.B. & Horsfield W.T. 1974. West Spitsbergen orogen. *Geological Society Special Publication 4*, 747–755.

Irvine T.N. & Baragar W.R.A. 1971. A guide to chemical classification of the common volcanic rocks. *Canadian Journal of Earth Sciences 8*, 523–548.

Jackson H.R., Forsyth D.A. & Johnson G.L. 1986. Oceanic affinities of the Alpha Ridge, Arctic Ocean. *Marine Geology 73*, 237–261.

Jokat W. 2003. Seismic investigations along the western sector of Alpha Ridge, central Arctic Ocean. *Geophysical Journal International 152*, 185–201.

Jones S.F., Wielens H., Williamson M.C. & Zentilli M. 2007. Impact of magmatism on petroleum systems in the Sverdrup Basin, Canadian Arctic Islands, Nunavut: a numerical modelling study. *Journal of Petroleum Geology 30*, 237–256.

Kelley S. 2002. Excess argon in K–Ar and Ar–Ar geochronology. *Chemical Geology 188*, 1–22.

Kontak D.J., Jensen S.M., Dostal J., Archibald D.A. & Kyser T.K. 2001. Cretaceous mafic dyke swarm, Perry Land, northernmost Greenland: geochronology and petrology. *Canadian Mineralogist 39*, 997–1020.

Kos'ko M.K. & Trufanov G.V. 2002. Middle Cretaceous to Eopleistocene sequences on the New Siberian Islands: an approach to interpret offschore seismic. *Marine and Petroleum Geology 29*, 901–919.

Le Bas M.J., Le Maitre R.W., Streckeisen A. & Zanettin B. 1986. A chemical classification of volcanic rocks based on the total alkali–silica diagram. *Journal of Petrology 27*, 745–750.

Ludwig K.R. 2008. *User's manual for Isoplot 3.7. A geochronological toolkit for Microsoft Excel. Berkeley Geochronology Center Special Publication 4*. Berkeley, CA: Berkeley Geochronology Center.

Maher H.D. Jr. 2001. Manifestation of the Cretaceous High Arctic Large Igneous Province in Svalbard. *Journal of Geology 109*, 91–104.

Maher H.D. Jr. & Craddock C. 1988. Decoupling as an alternative model for transpression during the initial opening of the Norwegian Greenland Sea. *Polar Research 6*, 137–140.

Menand T. 2008. The mechanics and dynamics of sills in layered elastic rocks and their implications for the growth of laccoliths and other igneous complexes. *Earth and Planetary Science Letters 267*, 93–99.

Meschede M. 1986. A method of discriminating between different types of mid-ocean ridge basalts and continental tholeiites with the Nb–Zr–Y diagram. *Chemical Geology 56*, 207–218.

Mukasa S.B., Andronikov A., Mayer L.A. & Brumley K. 2009. Submarine basalts from the Alpha/Mendeleev Ridge and Chukchi Borderland: geochemistry of the first intraplate lavas recovered from the Arctic Ocean. *Geochimica et Cosmochimica Acta 73*, A912.

Ntaflos T. & Richter W. 2003. Geochemical constraints on the origin of the Continental Flood Basalt magmatism in Franz Josef Land, Arctic Russia. *European Journal of Mineralogy 15*, 649–663.

Ogg J.G., Ogg G. & Gradstein F.M. 2008. *The concise geologic time scale*. Cambridge: Cambridge University Press.

Parker J.R. 1966. Folding, faulting and dolerite intrusiona in the Mesozoic rocks of the fault zone of central Spitsbergen. *Norsk Polarinstitutt Årbok 1964*, 47–55.

Parker J.R. 1967. The Jurassic and Cretaceous sequence in Spitzbergen. *Geological Magazine 104*, 487–505.

Pearce J.A. & Cann J.R. 1973. Tectonic setting of basic volcanic rocks determined using trace element analyses. *Earth and Planetary Science Letters 19*, 290–300.

Pearce J.A. & Norry M.J. 1979. Petrogenetic implications of Ti, Zr, Y, and Nb variations in volcanic rocks. *Contributions to Mineralogy and Petrology 69*, 33–47.

Pearce T.H., Gorman B.E. & Birkett T.C. 1977. The relationship between major element chemistry and tectonic environment of basic and intermediate volcanic rocks. *Earth and Planetary Science Letters 36*, 121–132.

Sambridge M.S. & Compston W. 1994. Mixture modeling of multi-component data sets with application to ion-probe zircon ages. *Earth and Planetary Science Letters 128*, 373–390.

Saunders A.D. 2005. Large igneous provinces: origin and environmental consequences. *Elements 1*, 259–263.

Shervais J.W. 1982. Ti–V plots and petrogenesis of modern and ophiolitic lavas. *Earth and Planetary Science Letters 59*, 101–118.

Silantyev S.A., Bogdanovskii O.G., Fedorov P.I., Karpenko S.F. & Kostitsyn Y.A. 2004. Intraplate magmatism of the De Long Islands: a response to the propagation of the ultraslow-spreading Gakkel Ridge into the passive continental margin in the Laptev Sea. *Russian Journal of Earth Sciences 6*, 1–31.

Smith D.G., Harland W.B., Hughes N.F. & Pickton C.A.G. 1976. The geology of Kong Karls Land, Svalbard. *Geological Magazine 113*, 193–232.

Steiger R.H. & Jäger E. 1977. Subcommission on geochronology: convention on the use of decay constants in geo- and cosmochronology. *Earth and Planetary Science Letters 36*, 359–362.

Sun S.-S. & McDonough W.F. 1989. Chemical and isotopic systematics of oceanic basalts: implications for mantle composition and processes. In A.D. Saunders & M.J. Norry (eds.): *Magmatism in the ocean basins*. Pp. 313–345. London: The Geological Society/Blackwell Scientific Publications.

Sweeney J.F. 1985. Comments about the age of the Canada Basin. *Tectonophysics 114*, 1–10.

Talvani M. & Eldholm O. 1977. Evolution of the Norwegian–Greenland Sea. *Geological Society of America Bulletin 88*, 969–999.

Tarakhovskiy A.N., Fishman M.V., Shkola I.V. & Andreichev V.L. 1982. Vozrast trappov Zemli Frantsa-Iosifa. (Age of traprocks of Franz Josef Land). *Doklady Akademii Nauk SSSR 266*, 965–969.

Tarduno J.A. 1998. The High Arctic Large Igneous Province. In: *Third International Conference on Arctic Margins, Celle,*

Germany. Abstracts. P. 184. Hannover: Bundesanstalt für Geowissenschaften und Rohstoffe.

Trettin H.P. & Parrish R. 1987. Late Cretaceous bimodal magmatism, northern Ellesmere Island: isotopic age and origin. *Canadian Journal of Earth Sciences 24*, 257–265.

Vincenz S.A., Cossack D., Duda S.J., Birkenmajer K., Jelenska M., Kadzialko-Hofmokl M. & Kruczyk J. 1981. Palaeomagnetism of some late Mesozoic dolerite dykes of South Spitsbergen. *Geophysical Journal of the Royal Astronomical Society 67*, 599–614.

Vincenz S.A., Jelenska M., Aiinehsazian K. & Birkenmajer K. 1984. Palaeomagnetism of some late Mesozoic dolerite sills of east central Spitsbergen, Svalbard Archipelago. *Geophysical Journal of the Royal Astronomical Society 78*, 751–773.

Citation: *Polar Research* 2011, *30*, 7306, DOI: 10.3402/polar.v30i0.7306